DESIGN AND ANALYSIS OF HIGH POWER LASER SYSTEMS

TSANG KWONG SHING

Ph.D

The Hong Kong Polytechnic University

2017

The Hong Kong Polytechnic University

Department of Electronic and Information Engineering

Design and Analysis of High Power Laser Systems

Tsang Kwong Shing

A thesis submitted in partial fulfilment of the requirements for the degree of Doctor of Philosophy

September 2014

CERTIFICATE OF ORIGINALITY

I hereby declare that this thesis is my own work and that, to the best of my knowledge and belief, it reproduces no material previously published or written, nor material that has been accepted for the award of any other degree or diploma, except where due acknowledgement has been made in the text.

_____ (Signed)

Tsang Kwong Shing (Name of student)

Dedication

To my supervisor, co-supervisor, my family and all my friends

Motto

To learn and to apply, for the benefit of mankind

Abstract

The thesis entitled “Design and Analysis of High Power Laser Systems”, aims to study how to design, develop and analysis compact, reliable, efficient, and cost-effective high power fiber lasers. Different from other kinds of laser, fiber lasers can provide a very small beam spot and the beam diameter can be only a few several microns. Therefore, these fiber lasers can be used in different areas especially in industrial applications such as telecommunication, laser marking, laser cutting, optical sensing, etc.

In telecommunication industry, new optical fiber networks such as CATV systems with passive optical network (PON) are commonly deployed. As a result, single mode fibers carrying several watts of optical power is used instead of multimode fibers. High power lasers can be achieved by using high power EDFAs. New technologies including double cladded fibers (DCFs), and pump combiner are used. Besides passive components, practical skills such as cladding pumping, and cladding mode stripping will be discussed.

We will consider both continuous wave (CW) as well as pulse lasers. Pulse lasers by using waveguide ring resonators in passive mode-locking would also be analyzed. Use of ring resonator is a modern technology to build ultrashort pulse lasers. The pulse lasers can be used in high fiber laser systems as seed

laser.

The thesis is divided into three parts. Chapter 1 introduces the laser mechanism. Studies of the structures and characteristics of lasers including single frequency operation, narrow linewidth, and measurement of laser noise are also included. A narrow linewidth 1064 nm fiber laser which can work in spectroscopy is introduced.

In Chapter 2, we discussed high power fiber amplifiers, including the designs, constructions, operations, and limitations of high power fiber amplifiers. Wideband fiber amplifier in 1 μm range is report. The amplifier can work with the fiber laser mentioned in Chapter 1 in order to provide a high output power. Also, demonstration in LiDAR sensing application is given.

Chapter 3 discussed pulse lasers, including advanced passive mode-locking by using waveguide ring resonators. Stabilizing of mode-locked laser is demonstrated. Also, 2 μm range mode-locked laser by using mircoring resonator is reported. The progress as well as further development is given on Chapter 4.

Publications Arising from the Thesis

Conference papers:

1. **K.S. Tsang**, Jie Wang, Li Jin, Victor Ho, Jack Cheung, Yanny Tsang, Alessia Pasquazi, Ray Man, Sai T. Chu, A. Ping Zhang, H.Y. Tam, and P. K. A. Wai, “1.8 μm High-Order Microring Resonator Mode-locked Laser Using a Carbon Nanotube”, OECC Publication Year: 2016
2. **K.S. Tsang**, Li Jin, Victor Ho, Jack Cheung, Alessia Pasquazi, Ray Man, Sai T. Chu, and P.K.A. Wai (2015, November). “Passive Mode-Locking at 1.8 μm using a High-Order Microring Resonator in a Figure Eight Fiber Laser”, Asia Communications and Photonics Conference (pp. AM3B-6). Optical Society of America.
3. Lin Jin, Alessia Pasquazi, **K.S. Tsang**, Victor Ho, Marco Peccianti, Lucia Caspani, Marcello Ferrera, E.Y.B. Pun, P.K.A. Wai, Brent E. Little, David J. Moss, Roberto Morandotti, and Sai T. Chu, “Burst-mode operation of a 650GHz mode-locked laser based on a high order microring resonator”, Optical Fibre Technology, 2014 OptoElectronics and Communication Conference and Australian Conference on Publication Year: 2014, Page(s): 70 - 72

4. **K.S. Tsang**, Ray Man, H.Y. Tam, C. Lu, P.K.A. Wai, “Optimal Design of Double-Clad Ytterbium-Doped Fiber Amplifiers Operating at 1020-1070 nm” Lasers & Electro Optics & The Pacific Rim Conference on Lasers and Electro-Optics, 2009. CLEO/PACIFIC RIM '09. Conference on DOI: 10.1109/CLEOPR.2009.5292557
5. **K.S. Tsang**, Ray Man, L.Y. Shao, H.Y. Tam, C. Lu, P.K.A. Wai, “Single-frequency single-polarization fiber ring laser at 1053 nm”, Opto-Electronics and Communications Conference, 2008 and the 2008 Australian Conference on Optical Fibre Technology. OECC/ACOFT 2008. Joint conference of the DOI: 10.1109/OECCACOFT.2008.4610339 Publication Year: 2008 , Page(s): 1
6. **K.S. Tsang**, Ray Man, P.K.A. Wai, H.Y.Tam, “Single frequency Ytterbium doped fiber ring laser without mode hoping”, The 8th IEEE Hong Kong Lasers & Electro-Optics Society (LEOS) Postgraduate Conference will be held at the Hong Kong Polytechnic University on 8th December, 2007.

Acknowledgements

I would like to express my sincere gratitude to my supervisor, Prof. Ping-kong Alexander Wai, and co-supervisor, Dr. Wai-sing Man. Their insightful direction, patient guidance, advices, discussion, and encouragement are invaluable.

I sincerely thank Prof. H.Y. Tam, Dr. S.T. Chu, Dr. C.Y. Li, Dr. F. Li, Dr. Dick Chung, Dr. Kevin Lui, and Dr. Shaohao Wang for sharing their extensive knowledge and for giving valuable advices.

Thanks to other members of Photonics Research Centre and the staff of the Department of Electronic and Information Engineering and the Department of Electrical Engineering for their support.

Last but not least, I would like to thank Amonics Limited for the support of this work.

Statement of Originality

The following contributions reported in this thesis are claimed to be original.

1. I design the 1053 nm single frequency single polarization narrow linewidth laser by using three level filters approach.
2. I demonstrate the measurement of laser linewidth and RIN noise.
3. I design a wideband fiber amplifier operating at 1020 to 1080nm range with small gain variation.
4. I demonstrate the use of LDF DCF and MFA, and the application in wind speed detection by using a nanosecond pulse fiber laser system.
5. I design the advanced pump dump design by applying double pump dumps with bending radius.
6. I demonstrate the repetition rate stability enhancement by using TEC and PZT fiber loop control.
7. I suggest the use of microring resonator in 2 μm range passive mode-locking fiber laser.
8. I determine the ring resonator and figure-eight effect in the mode-locked laser by using numerical simulation with SA effect.

Table of Contents

Chapter 1 Introduction

Laser stands for “Light Amplification by Stimulated Emission of Radiation”. The key structure is an optical resonator, which is a laser cavity having a gain medium in between two reflectors. When the gain is larger than the loss inside the cavity, the gain medium can amplify the circulating light. A stimulated emission of light is obtained after a number of roundtrips. Laser is a light source with properties such as coherence and very narrow spectrum.

The most common gain media include gas and solid state. Gas lasers such as CO_2 lasers are commonly used in marking and cutting. However, the beam quality and the size of gas lasers are not as good as solid state lasers. For solid state lasers, the gain media are made by glass or crystal. Fig. 1 shows a typical end pumped solid state laser. The pumping source is a diode at a shorter wavelength, which is normally at a high power but low beam quality. To launch the optical pumping into the gain medium, end pumped or side pumped is the most common pumping method. The optical resonator can be constructed by using a pair of mirrors: high reflection (HR) mirror and output couple (OC) mirror. The HR mirror allows the pump light to pass through the mirror while reflects the lasing wavelength back to the cavity. The OC mirror reflects part of the light while the rest would pass through. Lens may be used to focus the pumping light or the output light.

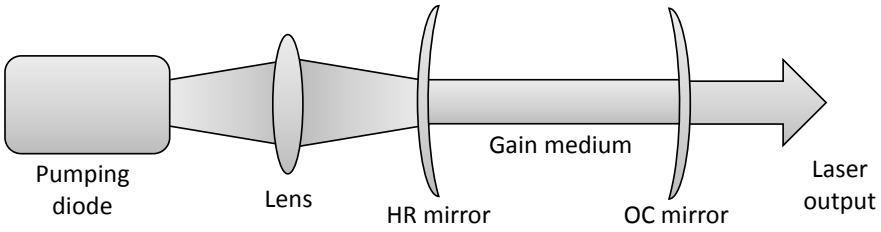

Fig.1. Typical end pumped solid state laser

This Chapter is going to review fiber lasers, including laser structure and laser properties. Fiber lasers can emit with different properties under different structures, such as single frequency, narrow linewidth, etc. Laser light can propagate over long distance without much divergence. In addition, fiber lasers can be CW or pulses in femtosecond to picosecond range. Pulse operation will be discussed Chapter 3.

1.1 Fiber lasers

Fiber lasers are a kind of solid state lasers. Doped fibers are used as the gain medium within a cavity. The first fiber laser is invented in 1962 [1], which used neodymium (Nd^{3+}) doped fiber as the active gain medium. Then, fiber lasers developed quickly afterwards. Fiber lasers in general have good beam quality, high conversion efficiency, and stable operating performance.

We can use fibers to build lasers or fiber amplifiers. In general, a laser system using a solid state DFB laser as a seed laser and then amplifies with fiber amplifier can be called a fiber laser system as well. In the other words, part of a laser system using fiber to build either the seed laser or amplifier can also be called a fiber laser.

As mentioned, fiber lasers are lasers using optical fibers as gain media, which are active fibers doped with rare earth ions such as erbium (Er^{3+}), neodymium (Nd^{3+}), ytterbium (Yb^{3+}), thulium (Tm^{3+}), or praseodymium (Pr^{3+}).

Laser diodes, or semiconductor lasers, are the most common solid state laser. Single mode laser diodes can provide output power up to around 1 W while multimode laser diodes can provide up to around kilo-watts. By using single mode laser diodes, the pump light can be coupled into active fiber cores directly. For high power fiber lasers using double cladded fibers, the pump light is coupled into the

fiber inner cladding. The details will be discussed in the next Chapter.

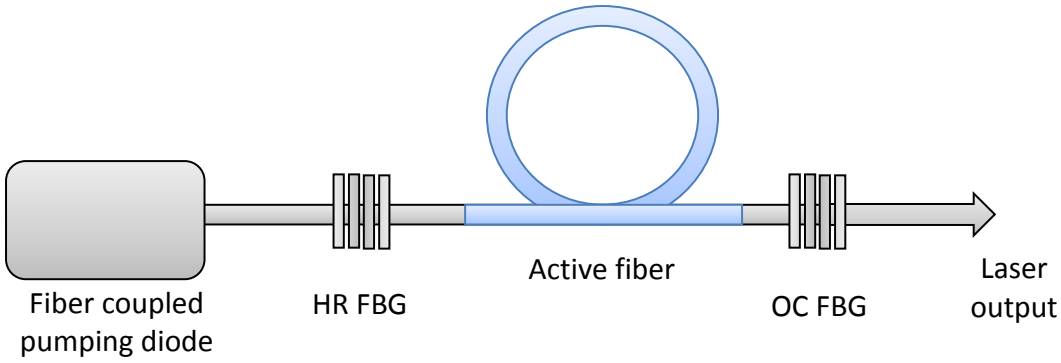

Fig.2. Setup of a simple fiber laser.

Fig. 2 shows a simple fiber laser setup by using fiber Bragg gratings (FBGs). Pump light is coupled into the fiber. The light is then launched into the core of the active fiber (rare earth doped fiber) by passing through a HR FBG. The generated light then reaches the OC FBG. Some of the generated light is reflected back to the fiber while part of light exits to the right after passing through the OC FBG.

A linear or ring cavity can be used to form a laser resonator. In case of a linear cavity, reflectors are used. There are different types of reflectors used in linear fiber laser resonators.

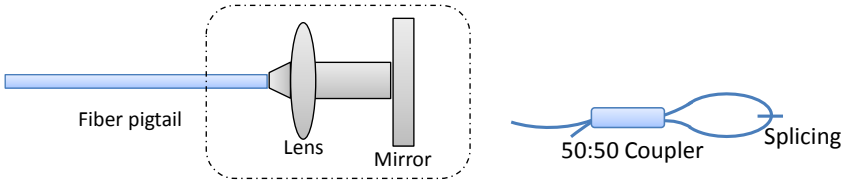

Fig.3a. Fiber mirrors. Fiber mirror (Left), fiber loop mirror (Right).

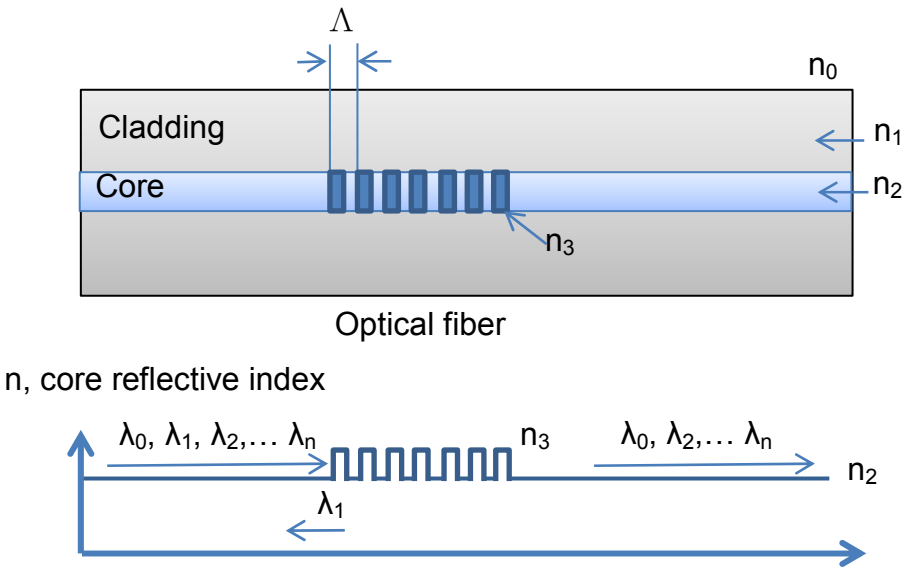

Fig.3b. A FBG Reflector

Fig. 3a shows a free space fiber mirror and a fiber loop mirror. The mirrors can reflect all the signal input. Fig. 3b shows a FBG, which is also commonly used in fiber laser. λ_1 is the Bragg wavelength, which is given by

$$\lambda_1 = 2\, n_3 \Lambda, \qquad (1)$$

where n_3 is the effective refractive index of the grating in the fiber core and Λ is the grating period. The wavelength bandwidth, $\Delta\lambda$, is given by

$$\Delta\lambda = [2(n_3-n_2)\,\eta/\pi]\,\lambda_1, \qquad (2)$$

where η is the fraction of power in the fiber core. Normally, FBGs are used in high power fiber lasers. There are three main reasons. First, there is no additional passive component and FBGs have low loss because they are fiber based. Second, the laser bandwidth and wavelength can be selected by choosing the proper FBGs. Third, OC FBGs allow selection of the percentage of reflection easily. AR coating or additional processing is not needed.

Besides linear cavity, ring cavity can be used to build fiber lasers. An isolator which allows light to pass through in one direction only is added to the ring cavity space. The advantage of unidirectional cavity is its ability to reduce non-linear effects such as spatial hole burning (SHB).

Disadvantages of fiber lasers

Fiber lasers have several disadvantages. First, it is difficult to build a fiber laser with cavity length less than one meter. Thus, it is difficult to achieve single frequency lasers and high repetition rate mode-locked lasers. The repetition can hardly reach over 100 MHz.

In normal single mode fibers, the fiber devices may be bifringent. The

polarization state of light may change from linear to elliptical. The changes depend on temperature and fiber bending. Therefore, fiber lasers may require adjusting the polarization by using polarization controllers from time to time. Polarization maintaining (PM) fibers can be used to eliminate the problem.

Advantages of fiber lasers

High efficiency high output power is an important characteristic of fiber lasers. The limit is about several kilowatts with double cladded fibers. Other advantages include compactness, large gain bandwidth, wide wavelength tuning range, and ability to generate ultrashort pulses.

The exact pump wavelength is not critical since fiber lasers have broad pump absorption spectra. As a result, a wide operation temperature range of the pump diodes is acceptable. Another important property is good beam quality if single mode fibers are used. Fiber lasers in general have high beam quality at all power levels, which is not the case for other lasers. Finally, the fiber acts as a waveguide making alignment unnecessary which is not the case for free space lasers.

1.2 Single frequency operation

Single frequency lasers are lasers operating with only one single cavity mode. The main characteristic of single frequency fiber lasers is very narrow linewidth. It can reach only a few kilohertz. Therefore, the coherence length is long.

A number of laser applications required lasers with single frequency, including coherent communications, wavelength division multiplexing systems, high resolution atomic and molecular spectroscopy, and laser interferometer gravitational wave detection [2-5]. In the meantime, linear polarization and narrow linewidth are essential in some of these application [6].

Types of single frequency Lasers

The first type of single frequency lasers is distributed feedback (DFB) lasers, distributed Bragg reflector (DBR) lasers, and external cavity laser diodes. A specific frequency is selected in the cavity. Typical linewidths of DFB lasers and DBR lasers are in the megahertz range. DFB lasers with special designs such as using narrow band FBG can reduce the linewidth down to hundreds of kilohertz. Typical linewidth of external cavity laser diodes is about a hundred kilohertz.

The second type of single frequency lasers is vertical cavity surface emitting lasers (VCSELs). Vertical cavity can provide a short laser gain resonator and large

cavity mode spacing. Thus, it can only emit one single mode. Since the resonator is short, the output power can only reach a few milli-watts, and the linewidth is in the megahertz range.

The third type is fiber lasers. Since the cavity length of fiber lasers is long, the cavity spacing is narrow. Therefore, there are many cavity modes in fiber lasers. In order to achieve single frequency operation, special methods are required to reduce the number of cavity modes. Different forms of filters are deployed, such as narrow band FBGs, or un-pumped active fibers. The output power can reach up to a few tens of milli-watts. The details will be discussed later.

Single frequency lasers and mode hopping

As mentioned, one way to allow single frequency operation is to have a gain bandwidth smaller than the cavity mode spacing. Then, the laser can only operate in one single cavity mode. Therefore, single frequency lasers usually use short cavities to increase the mode spacing. Otherwise, optical filters can be used to reduce the number of modes inside the cavity.

When a laser operates under single frequency, it may first operate in one single cavity mode, but jump to another cavity mode suddenly, which is called mode hopping. Mode hopping is often caused by external factors, such as temperature drift.

Since the fiber cavity is long and the mode spacing is narrow, mode hopping can be easily found in fiber lasers than other types of single frequency lasers.

For example, if there is a temperature drift, it would cause both passive and active fiber length drifts. If the passive fiber length drifts within the cavity, the mode frequencies are shifted without changing the gain profile. If the active fiber length drifts, there may be wavelength shifts for both the maximum gain and the frequencies of the resonator modes. The lasing frequency will change if another mode obtains a higher gain than the current lasing mode because of the shift.

Construction of single frequency fiber laser

It is difficult to achieve stable single frequency fiber laser because there is mode competition among different longitudinal modes and polarization modes. We proposed a laser configuration and demonstrated a 1053 nm single frequency fiber ring laser without mode hopping.

Through the use of polarization maintaining 980 fibers (PM 980) for the active cavity and the saturable absorber, the configuration enables the realization of a narrow linewidth single frequency fiber laser with linewidth less than 10 kHz. The fiber laser reported here is shown schematically in Fig. 5. The gain fiber is a PM YDF with 10 m fiber length. In order to achieve narrow linewidth operation, a PM YDF is

used as the saturable absorber (SA). The fiber length is 2 m. A 500 mW pump laser is used. The operating wavelength of the pump laser is 975 nm. A pair of cascaded FBGs is used for the filtering function. The reflection coefficient of FBG 1 is the same as the reflection coefficient of FBG 2. The reflective rates are 80%. The length, L, between these two FBGs is 0.01 m. The total cavity length is about 15 m. The corresponding mode spacing is about 13 MHz.

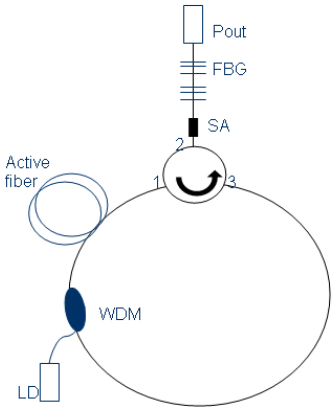

Fig. 5. Diagram of the fiber ring laser

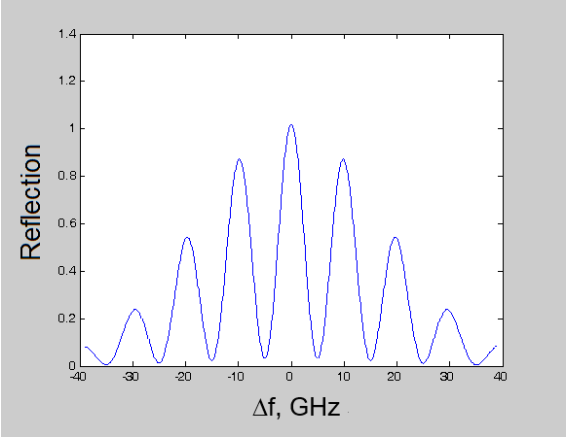

Fig. 6. Reflection of the cascaded FBGs

For laser operating at 1053 nm, a 0.2 nm grating would be about 54 GHz wide, therefore a single FBG is not enough to eliminate all the modes. Cascading two FBGs will result in etalon effect thus enhancing the filtering required for the fiber laser [4]. Using the following equation from [5]

$$R = r1 + r2 + 2(r1r2)^{1/2}\cos\phi \quad , \tag{3}$$

where r1 and r2 are the reflection coefficients of FBG 1 and FBG 2 respectively, and

$$\cos\phi = 4\pi nL / \lambda \quad , \tag{4}$$

is the reflection caused by the cascaded FBG filters which can be calculated as shown in Fig. 6. The filter can suppress the mode competition by restricting the number of modes in the ring laser

Further filtering is needed to realize single mode operation, which is achieved through an un-pumped YDF as a saturable absorber. It also can act as a narrow bandpass filter [2-3]. To optimize the filtering effect and to balance the gain in the cavity, an optimum length of the SA and the pump power should be selected [7]. The longer the length of the YDF, the narrower the bandwidth of the bandpass filter will be. However, polarization variation will result in SHB if a non-PM YDF is used [6]. In addition, the bandwidth of the filter is affected the pump power as well [6].

PM fibers are used for the cavity and the SA is used to eliminate the effect of polarization. Although alternative methods to suppress SHB such as by using a polarization controller or a PM SA together with a polarizer have been proposed before. However, they can only realize short term stability since the birefringence of non-PM fibers can easily be perturbed by environmental conditions.

These techniques together with the optimization of system parameters enable us to realize a stable single frequency fiber ring laser.

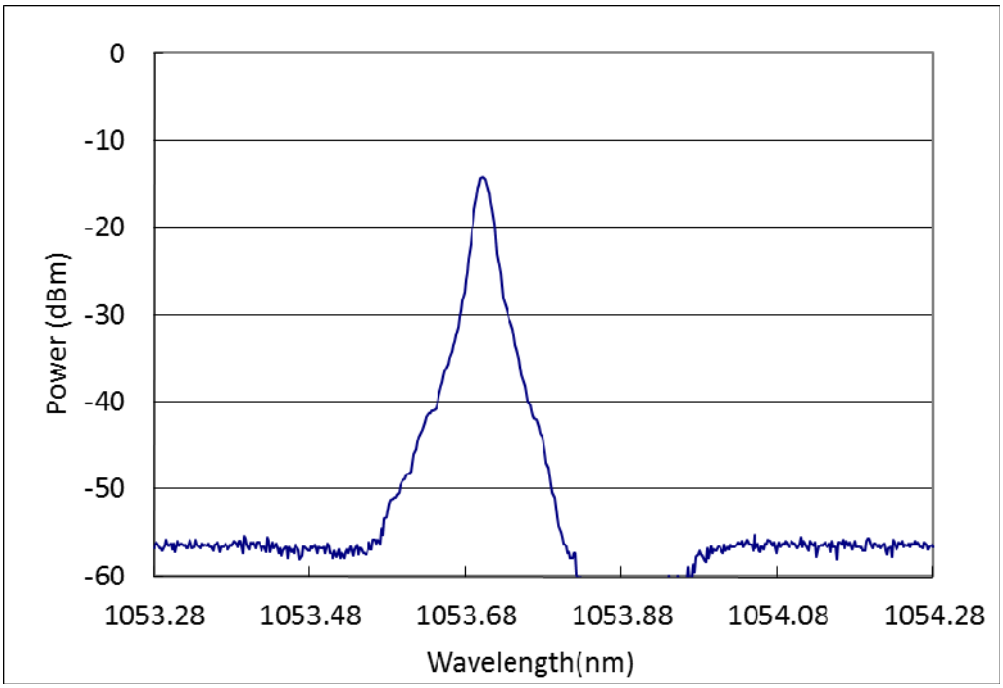

Fig. 7a. Measured optical spectrum

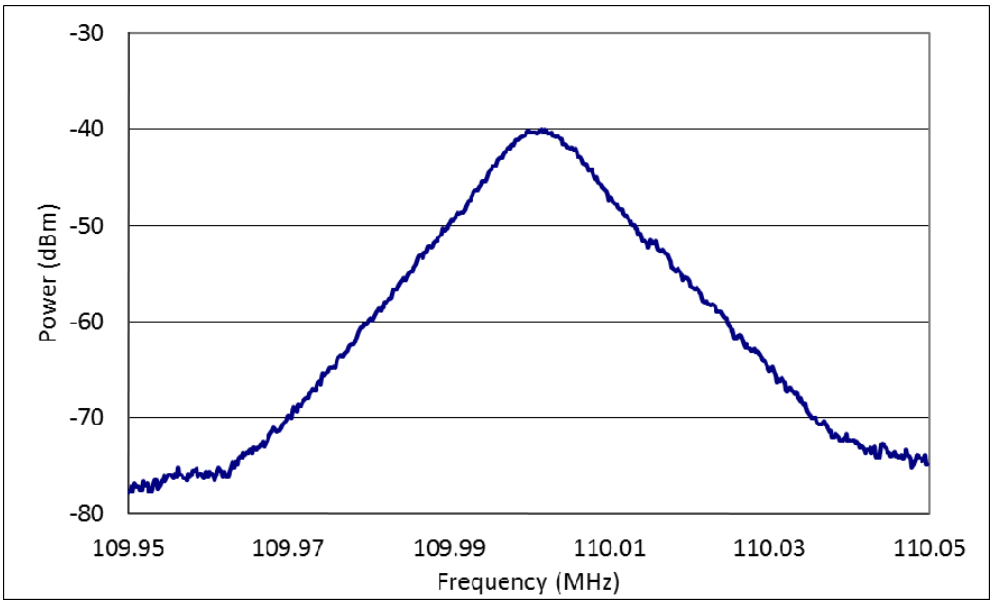

Fig. 7b. Measured linewidth

Fig. 7a shows the spectrum measured using an optical spectrum analyzer (OSA) at the output port by adding a 1:99 tap coupler. The 1% output port of the tap coupler is measured. The total output power is about 10 dBm with 1053.78 nm center wavelength. The measurement using an electrical spectrum analyzer (ESA)

confirmed single frequency operation of the laser. Self-heterodyne linewidth measurement is carried out. The result is shown in Fig. 7b. By considering the -20 dB measured full width, the linewidth of the laser is less than 10 kHz. The linewidth measurement will be shown in the next Section.

1.3 Laser noise

There are two types of laser noise, which are intensity noise and optical frequency noise. Intensity noise is the fluctuation of optical intensity, and the measurement method is relative intensity noise, RIN. The interference between stimulated emission and spontaneous emission causes fluctuation in the optical intensity. Electrical signal demodulations are detected as beat noise. The intensity noise limits the system SNR. RIN is then normalized by the average optical power, expressed as per unit frequency, which can be shown as

$$RIN = \Delta N / P , \quad (5)$$

where ΔN is optical intensity noise, and P is average optical power. The measurement of RIN is direct. The laser source is coupled into a photodiode, and then the output RF signal is amplified by low noise amplifier before connecting to an ESA. The total electrical noise spectral density N_e can be defined as

$$N_e (f) = N_{Tn} + N_{Sn} + \Delta N, \quad (6)$$

where N_{Tn} is the thermal noise, and N_{Sn} is shot noise. From Eq (5), only the intensity noise is considered. Therefore, it is necessary to remove the thermal noise and the shot noise from the total noise power density measured by the detector.

Optical frequency noise is fluctuation in the optical frequency. First, the power spectrum density of the instantaneous frequency of the laser electric field is needed.

Then, the instantaneous frequency or time differentiation of the phase can be found.

Laser noise is due to the fluctuations of various parameters, which can be classified as quantum noise and technical noise. Quantum noise comes from the physical limit of the laser itself, particularly associated with spontaneous emission in the gain medium. Technical noise comes from excess noise of the pump source, vibration of the laser resonators, or temperature fluctuations.

Laser linewidth

Quantum noise is the physical limit of a laser linewidth. It can be calculated by using the Schawlow-Townes formula, which is given by

$$\Delta V_{laser} = \frac{\pi h\nu(\Delta\nu_c)^2}{P_{out}}, \tag{7}$$

where h is the Planck's constant, ν is the laser frequency, $\Delta\nu_c$ is the gain bandwidth, and P_{out} is the output power. From Eq. (7), the FWHM linewidth is related to the square of the gain bandwidth divided by the output power. A general form of the equation is given by

$$\Delta V_{laser} = \frac{h\nu\Theta l_{tot} T_{oc}}{4\pi T_{rt}^2 P_{out}}, \tag{8}$$

where T_{oc} is the output coupler transmission, l_{tot} is the total cavity losses, T_{rt} is the

cavity round trip time, and θ is the spontaneous emission factor.

The corresponding two-sided power spectral density of the phase noise is

$$S_{\varphi}(f) = \frac{h\nu\Theta l_{tot} T_{oc}}{8\pi^2 T_{rt}^2 P_{out}} f^{-2} \quad . \tag{9}$$

The corresponding white frequency noise is

$$S_{v}(f) = \frac{h\nu\Theta l_{tot} T_{oc}}{8\pi^2 T_{rt}^2 P_{out}} \quad . \tag{10}$$

It is difficult to achieve the Schawlow-Townes limit because there are different types of practical noise, such as vibrations of component mounting, temperature drifts, and pump power fluctuations.

From Eq. (7), fiber lasers with a long cavity have a small Schawlow-Townes linewidth. However, it is difficult to obtain stable single frequency operation without mode hopping in practice.

Laser linewidth measurement

Linewidth is measured by the electric field power spectrum of a laser. A single frequency fiber laser linewidth can be ~ kilohertz only. Therefore, it cannot be measured directly because the resolution for an OSA is not sufficiently high for measurement in the kilohertz range.

Linewidths larger than 0.01 nm, an OSA can simply be used. For laser with narrower linewidth, it is measured by the beat note between two lasers. In general, a reference laser with a noise level lower than that of the test laser source will be used.

To measure the linewidth of a single frequency fiber laser, self-heterodyne technique is used. It measures the beat note between the delayed laser output and the laser itself with a frequency shifted.

Self-heterodyne linewidth measurement

Since narrow linewidth cannot be measured directly by using an OSA, self-heterodyne is used for laser linewidth measurements.

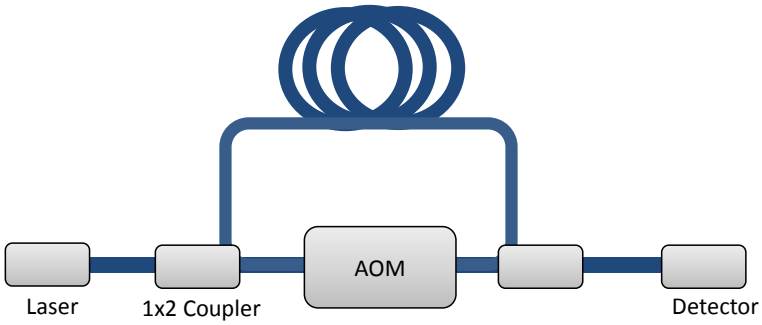

Fig. 8a. Self-heterodyne measurement setup

Fig. 8a is a basic self-heterodyne measurement setup. The laser output is divided into two paths. One path is coupled to an optical delay fiber. The other path is coupled to an acousto-optic modulator (AOM), which provides several tens of megahertz frequency shifts. The two paths are then combined using another coupler,

thus, the two light beams superimpose. A photo detector records the resulting beat note, which is located at the AOM shifted frequency. The laser linewidth can then be determined.

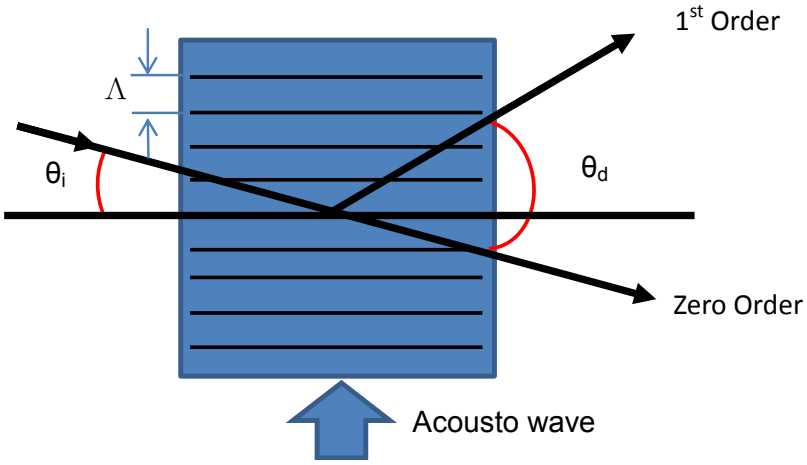

Fig. 8b. Construction of an AOM

Fig. 8b shows the construction of an AOM. The condition for constructive interference of the scattered light is

$$m\lambda = \Lambda(\sin\theta_i + \sin\theta_d), \qquad (11)$$

where m is an integer, Λ is the acoustic wavelength. θ_i is incident angle, and θ_d is deflected angle. From the Bragg condition, there is only one value for the deflection angle $\theta = 2\theta_d$. When $\theta_i = \theta_d$ and n=1, the acoustic beam system is optimized for the first order with maximum beam power. The corresponding angle is

$$\sin\theta_d = \lambda / 2\Lambda. \qquad (12)$$

Long delay lines are used in order to decorrelate the two lights. A self-convolution of the laser spectrum is measured. It is important to use a delay line longer than the coherence length. Special data processing is required when the laser

linewidth is narrow or when there is not enough delay fiber to obtain uncorrelated beams.

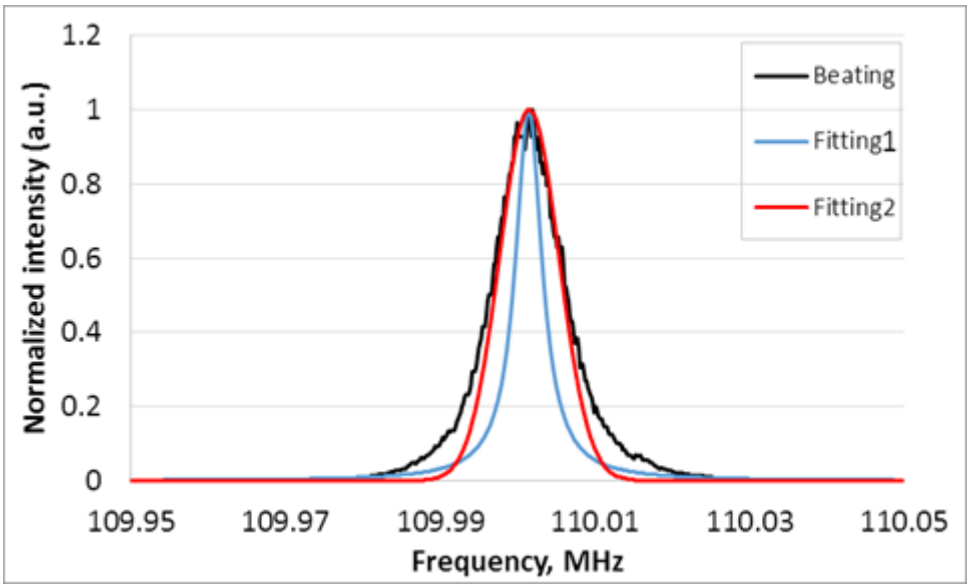

Fig.9. linewidth measurement (Fitting1 is a Lorentzian fit and Fitting2 is a Gaussian)

When we consider the fiber laser mentioned in the previous Section, the white noise of the laser is less than 1 mHz from Eq. (6). However, most narrow linewidth lasers contain a large amount of Gaussian noise, including pump noise, vibration noise, and acoustic noise, etc. As a result, a Voigt line is found, which includes both Gaussian and Lorentzian line. The 3 dB linewidth of the measured data, and the 3dB linewidth of the Gaussian fit are similar, at about 5 kHz. The 20dB linewidth of the Lorentzian fit is only about 2 kHz.

Gaussian fit represents the 1/f frequency noise and the white noise. The Lorentzian fit represents the white noise. The Lorentzian linewidth value is generally

smaller than the Gaussian linewidth in fiber lasers. It indicates that the 1/f frequency noise in low frequency range dominates the frequency noise.

From Fig. 9, the Lorentzian linewidth cannot be achieved from the linewidth fitting directly. The spectrum does not show the white noise level because the white noise from Eq. (6) is much lower. The Lorentzian linewidth or white noise can only be calculated from the optical noise spectrum with high frequency band larger than the megahertz range.

1.4 Conclusion

This Chapter is divided into two parts. The first part introduced the basic laser configuration, laser properties, and design parameters. The second part concentrated on the measurement of the laser noise, especially the frequency noise and linewidth. Laser noise and linewidth are two important factors. The measurement of intensity stability of laser sources will be discussed in Section 2.2.

The laser noise can be reduced in different ways. For example, we may reduce the quantum noise by increasing the intra-cavity power level and minimizing losses. We may also reduce the technical noise by stabilizing the laser resonators, and the temperature of the setup. Use of low noise pump sources can also reduce the technical noise.

We can optimize the laser parameters so that the laser is less affected by noise. We may consider laser setups which can suppress mode hopping, or use active or passive stabilization schemes. Suppression of mode hopping is demonstrated in the previous Section already. Long fiber cavity having narrow linewidth property is also achieved. Single frequency operation is achieved by reducing the number of cavity modes are also shown. Active stabilizing scheme will be used in Chapter 3 for stability improvement of pulse lasers. These approaches and methods are used and

discussed in Chapters 2 and 3.

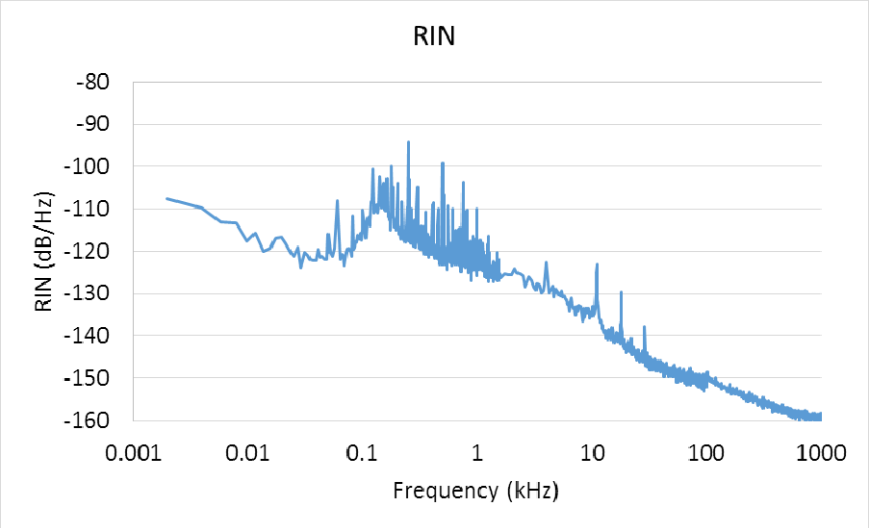

Fig.10a. RIN measurement after high power amplification

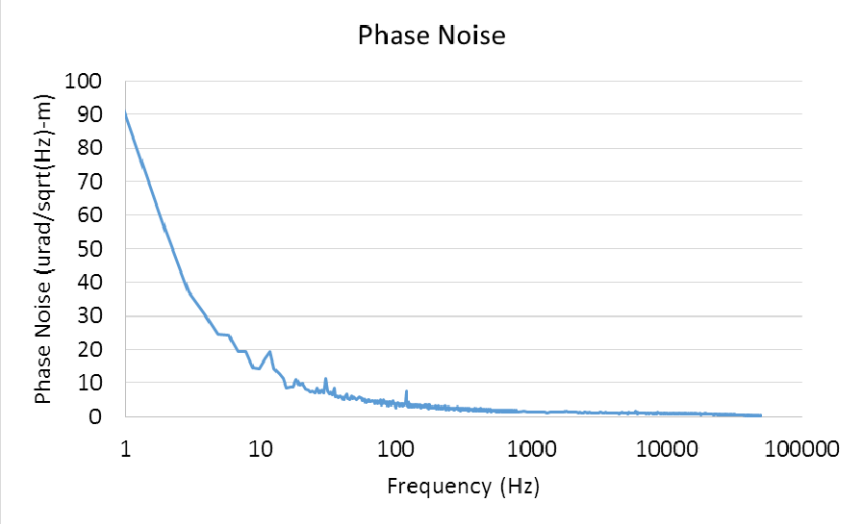

Fig.10b. Phase noise measurement after high power amplification

The RIN and phase noise of the laser are analyzed afterwards. Fig. 10a shows the RIN measurement after high power amplification. The data show there are noise peaks in 100 Hz to 1 kHz, which are not found in the laser source. The noise peaks are properly related to the electronic circuits. Modification of the electronic circuits is needed for improvement. Fig. 10b shows the phase noise measurement after fiber

amplification. Again, some small peaks are found. Further analysis is needed.

The proposed fiber laser can be used in spectroscopy, frequency conversion and medical treatments. There are many spectroscopy sensing applications in near infrared (NIR) range. Fig. 11 shows the NIR spectrum of liquid ethanol. We can measure the absorption of the laser source in order to estimate the percentage of the ethanol inside a liquid.

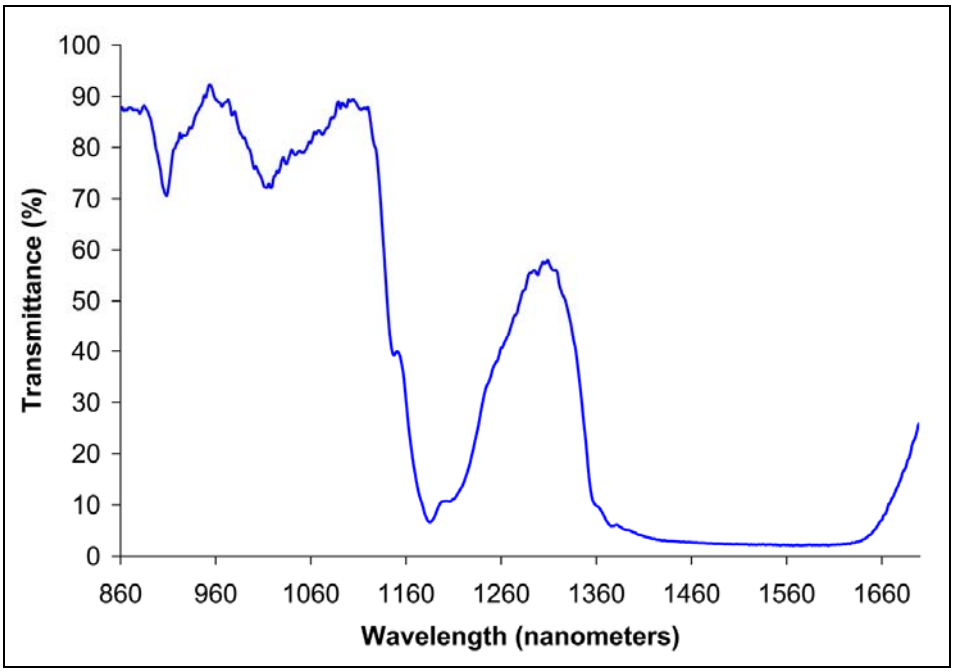

Fig.11a. Near-infrared spectrum of liquid ethanol (From wikimedia.org)

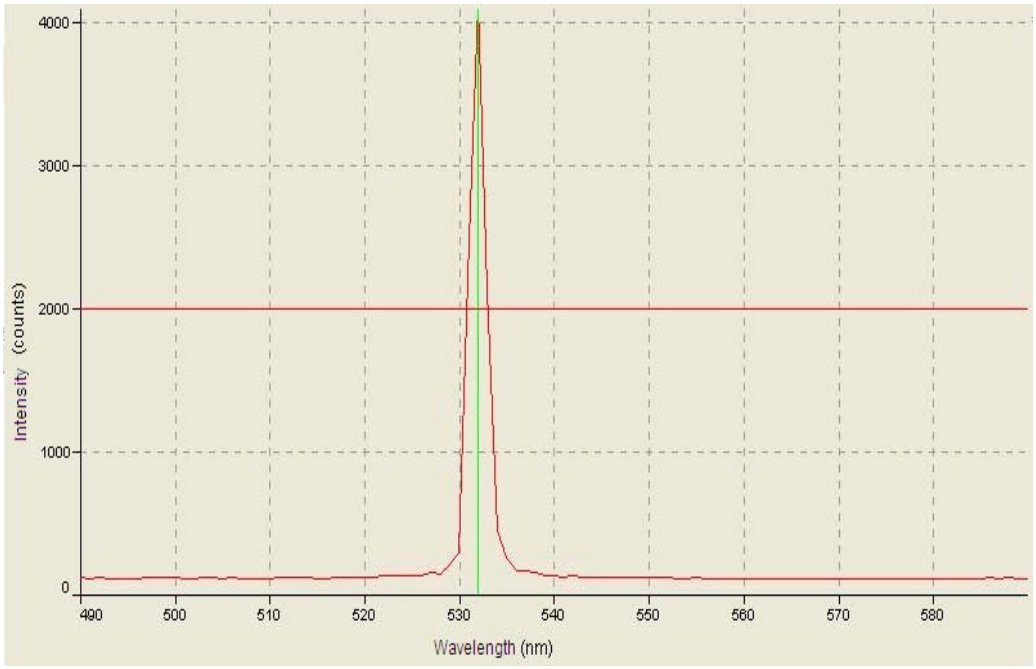

Fig.11b. Converted 532m output spectrum

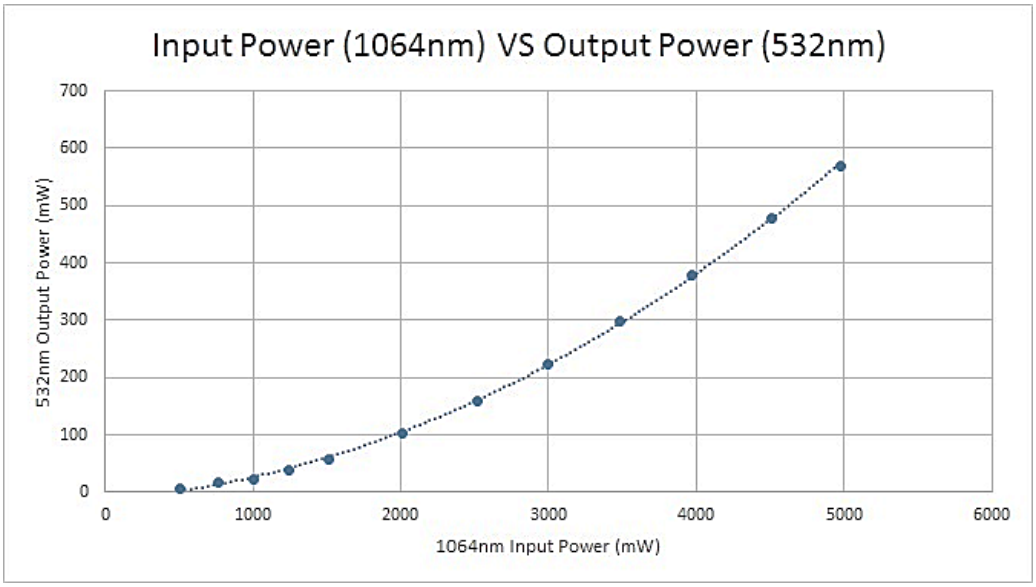

Fig.11c. Output power relationship of frequency conversion

Also, we can use the fiber laser in frequency conversion. A periodically poled lithium niobate (PPLN) is needed for frequency conversion. PPLN is a medium for nonlinear wavelength conversion processes. Frequency doubling can be carried out by using PPLN. Fig. 11a shows the converted 532 nm spectrum by using a 1064 nm

fiber laser. Fig. 11b shows the power relationship of the frequency conversion. A high output power narrow linewidth laser is required for the processes. In the next Chapter, we are going to study the high power fiber amplifier constructions.

Chapter 2 High power fiber amplifier

In order to achieve a high power fiber laser, a laser source is used together with a fiber amplifier, which is called master oscillator power amplifier (MOPA). Currently, rare earth doped double cladded fibers (DCFs) are commonly used to build high power fiber amplifiers [10]. A fiber core, an inner cladding, and an outer cladding can be found in a DCF. The fiber core is a single mode guiding the signal. The inner cladding is a multimode guiding the pump light.

To develop a high power fiber amplifier using DCFs, cladding pumping is required. The suitability and practicality of the pumping scheme should be considered. The factors include the linewidth of the input source, pump coupling efficiency, conversion efficiency, alignment sensitivity, splicing difficulty, compactness, and stability, etc. Therefore, we first review methods of building fiber lasers. Current researches concentrate on both the fiber structure as well as the pumping methods.

Rare earth doped DCFs are used in high power amplifiers because they can provide high single pass gain. In fact, the gain is the product of the pump intensity times the effective absorption length in the gain fiber. Within the effective absorption length, there is interaction between the input laser and the pumping in the gain fiber. Usually, Yb^{3+} doped DCF fibers can provide conversion efficiency up to

around 80%. In the next Section, the design and construction of Yb^{3+} doped DCF fiber amplifiers are demonstrated and studied.

High power fiber lasers can easily trigger fiber nonlinearities, such as stimulated Raman scattering (SRS) and four-wave mixing (FWM). Many researches have investigated these nonlinear effects [10, 11]. A larger core increases the threshold of triggering non-linear effects, however, it would also allow the propagation of higher order transverse modes.

In a conventional step index fiber, the maximum core diameter is about 10 μm in order to maintain a single transverse mode. Recently, large mode area (LMA) fiber is used to construct fiber lasers [11]. The fiber core diameter is larger than that of normal fiber. In order to maintain single mode operation, the numerical aperture (NA) is reduced by decreasing the refractive index difference between the core and the cladding. LMA fibers can reduce the power density of the fiber core. However, we have to be careful in handling LMA fibers in order to keep only one single transverse mode in the fiber core.

In addition, there are a number of technical issues when using DCF as a gain medium. First, the symmetry of the inner cladding may reduce the overlap between the pump and the input signal, and thus reduce the effective absorption length. As a result, it would enhance the thermal effect. Since the pump is absorbed in the fiber,

heat is generated. If the fiber is overheated, the cladding material would be degraded. Finally, the beam quality and the signal power would be reduced if the residual pump and the cladding signal are not treated properly.

In Section 2.2, the pulse amplification by using LMA DCF is demonstrated. Nanosecond pulse amplification is considered. Both physical limits, such as SBS and SRS, and practical limitations, including thermal, residual mode, etc, are considered.

2.1 Cladding pumping amplifier

Different types of laser structures as well as the laser properties have been discussed in the last Chapter. In this Section, we discuss high power lasers. Traditionally, single mode optical fibers and components cannot withstand high power. In order to achieve high output power, optical components are required to withstand high power as well.

High power fiber lasers pumped by high power multimode pump diodes through DCF was proposed in the 1970s. Fused couplers and combiners can handle high optical power because they are fiber based. Some optical components, such as isolators, filter WDM, and circulators are free space. Fiber ends are coupled to collimators inside the optical components. Adding end caps between the fiber ends and the collimators can reduce the power density. Thus, these optical components can handle higher optical power.

For different applications, the power level and laser quality requirements are different. Some high power lasers generate only few watts. However, for material processing, multiple kilowatts or at least a few hundred watts are required. Efficient heat management and removal are the main technical challenges in the generation of high powers.

For the laser qualities, the overall optical performances depend mainly on the seed lasers in MOPA systems. The parameters include laser linewidth, laser wavelength, beam quality, and pulse width, etc. For example, narrow linewidth high power MOPA fiber laser systems used in sensing applications would include narrow linewidth seed lasers and high power fiber amplifiers.

Double cladded fibers and beam quality

The power of single mode pump diodes is limited to about one watt or below. Multimode pump diodes can reach more than 10 W or even over 100 W. Although multimode fibers can withstand high power, the beam quality is poor. The use of double cladded fibers can take advantage of higher power multimode laser diodes as high power pumping sources.

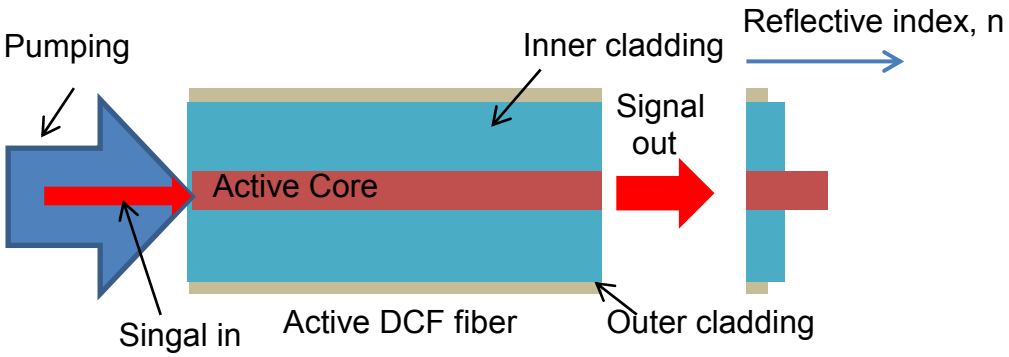

Fig.12. Schematic diagram of double cladded fibers.

Fig. 12 shows the launching of signal and pump light into the DCF. The pumping

light is coupled into the inner cladding, and the signal is coupled to the fiber core. The inner cladding is made of silica, and the outer cladding is commonly made of low index polymers. The NA of the core is low in order to maintain single mode. The typical M^2 is about 1.0 to 1.2. In Yb^{3+} doped DCF, the power efficiency is typically about 70%. The ratio of the areas of inner cladding and core cannot be too large to ensure high pump absorption. The area ratio is about 100 to 1000.

One disadvantage of double cladded fiber is the effective absorption length may be less than the actual fiber length. The pump light can propagate in the inner cladding and then exit the inner cladding. There is overlapping but not as much as single cladded fiber. Since the double cladded fiber we used is cylindrical symmetric, we enhance the pump absorption by periodically bending of the fiber.

Although asymmetric fiber structures such as D-shaped or rectangular pump cores have been used, these fibers are not commonly used in the industry since it is difficult to splice the fibers. The loss is significant for high power application. Since fusion splicer can recognize and align the core of symmetric fibers, the splicing loss is low and the splicing process is repeatable and reliable.

Launching the pump light and pump dumping

There are several common techniques to launch the pump light into double cladded fibers. End pump is one common technique based on pump combiner. Pump combiner is a device with DCF on one side fused together with several multimode fibers and one single mode fiber on the other side. Side pump is another technique used. It can be fiber coils side pumped, V-groove pump light injection, etc. Fiber coils side pumped is a method by wounding multimode fibers without coating around an active fiber without coating. Thus, the pump light can then be coupled into the active fiber.

When pump light is launched into a double cladded fiber, some of the pump power may get into the outer cladding around the pump cladding, and heat up the low index polymer coating. The low index polymer coating may then be damaged by excessive heating. Therefore, special care in splicing DCF, especially LMA DCF is essential if a pump combiner is used.

In a high power fiber amplifier using double cladded fibers, residual pump power and cladding signal should be considered. Residual pump means the unabsorbed pump power at the fiber end opposite to the pumping end. We have to remove the cladding signal and residual pump from the inner cladding. In forward pumping systems, the cladding light may mix with the output signal. In backward

pumping systems, the cladding signal may get into the signal source. A special cladding mode stripper should be used to remove the cladding signal.

Cladding mode stripper, or pump dump is a device to handle substantial optical powers. By removing the outer cladding of the double cladded fiber, high index jam is placed on the surface of inner cladding, which can remove the residual pump and cladding signal. Advanced pump dump, called cladding mode stripper is needed to keep the mode quality for LMA DCF because of its slightly multimode properties. The details about high power fiber amplifiers under pulse application are discussed in the next Section.

Wide range amplifier by using DCF and SCF

In this Section, we are going to use DCF to design a special amplifier. Usually, DCF is used to increase the pump power and the output power level. However, the emission profiles of DCF and SCF in Ytterbium doped fibers (YDFs) are different. Therefore, an optimal design of an YDF amplifier in the 1020 nm to 1070 nm range by using both SCF and DCF can be achieved.

The emission range of YDFs is broad, ranging from around 1.0 μm to around 1.1 μm. Spectroscopy, frequency conversion and medical treatments are the laser applications within the range. DCF YDFs can provide high efficiency, compactness,

and high reliability for lasers and amplifiers [12-14].

In short wavelength range less than 1040 nm, SCF should be considered instead of using DCF. The reason is the ytterbium transition is three-level in short wavelength range. Significant signal reabsorption in weakly pumped regions can be found easily in three-level transitions. As a result, YDF amplifiers for short wavelength should be achieved with SCF instead of DCF.

On the other hand, the ytterbium transition is predominately four-level for long wavelength higher than 1040 nm. Therefore, the gain is proportional to the overall upper-state population and the signal reabsorption is weak [14-15]. As a result, YDF amplifiers for long wavelength can be made by using DCF instead of SCF.

Amplifiers operating in 1020 nm to 1070 nm range are difficult to achieve, especially with a high gain and small gain variation. Amplifiers using DCF alone cannot cover the entire 1020 nm to 1070 nm range which by using only either SCF or DCF YDFs. In addition, the amplifier configuration is complex, the efficiency is low, and the gain variation may be large if only SCF is used [14].

Design the configuration

The schematic of the YDF amplifier utilizing both SCF and DCF YDFs is shown in Fig. 13. The amplifier consists of two parts, including a pre-amplifier stage and a booster stage. SCF is used as a pre-amplifier stage for the short wavelength range while DCF is used as a booster stage for the long wavelength range.

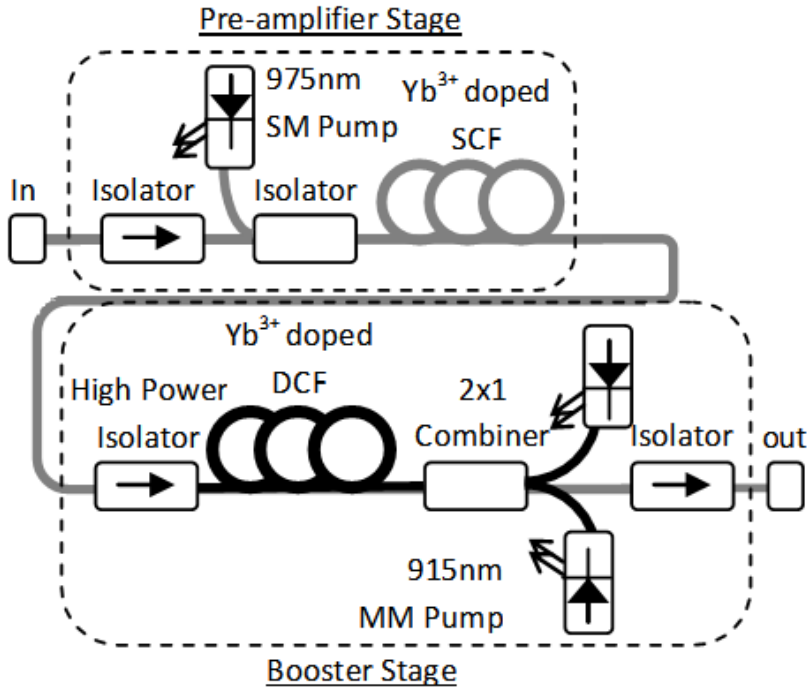

Fig.13. Configuration of the amplifier

A 600mW 975 nm pump is used in the SCF YDF pre-amplifier stage because 915 nm pumps have large amplified stimulated emission (ASE) noise. The ASE generated would limit the gain available at the long wavelengths [14]. The length of SCF YDF is 1.2 m. The gain achieved at 1020 nm is able to reach above 27 dB.

Two uncooled multimode 915 nm pump diodes are used in the booster stage

since the absorption bandwidth is wide at 915nm range. The pump absorption variation is low even the wavelength of the uncooled pump laser is changed due to the temperature changed. A combiner is used for cladding pumping with total 16 W maximum pump power. The optimized fiber length is 2.2 m. It is chosen carefully in order to reduce the reabsorption at 1020 nm. In addition, the gain drops as the length increases at 1020 nm as well. However, long fiber is essential to achieve high gain at 1070 nm.

Simulation and Experimental Result

In order to design an YDFA system, we carried out the simulation of SCF and DCF YDF amplifier by using a simulator provided by the fiber company. The simulator allows us to use different parameters, including the fiber length, pump power, and the signal inputs. We will then compare the results by building the YDFA and test the performances.

The simulated gain profiles of the amplifiers is shown in Fig. 14. Two profiles, only SCF and only DCF are given. The peak gain of SCF is found around 1030 nm, while the peak gain of DCF is found around 1070 nm. In addition, the profiles can show the operation range by using either SCF or DCF alone is narrow. Different gain curves can be achieved by using different pump powers or fiber lengths. However,

the required operation range cannot be obtained.

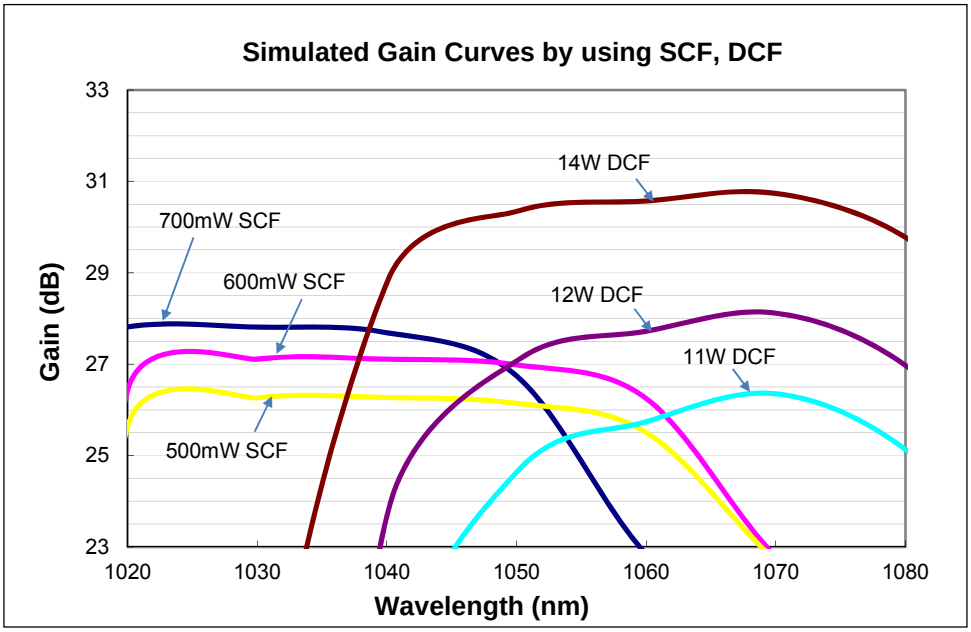

Fig.14. Simulated gain spectra of the SCF and DCF alone

The simulated and experimental measured results of the proposed amplifier are shown in Fig. 15. 28 dB gain with around 3 dB gain variation can be achieved by simulation in the wavelength range 1020-1070 nm. The experimental measured gain spectrum are shown in the cross points in Fig. 15. There are only limited number of measurements because of the limited available laser sources. However, the measured gain points match with the simulated results. The measured gain is 27 dB with a gain variation less than 1.83 dB.

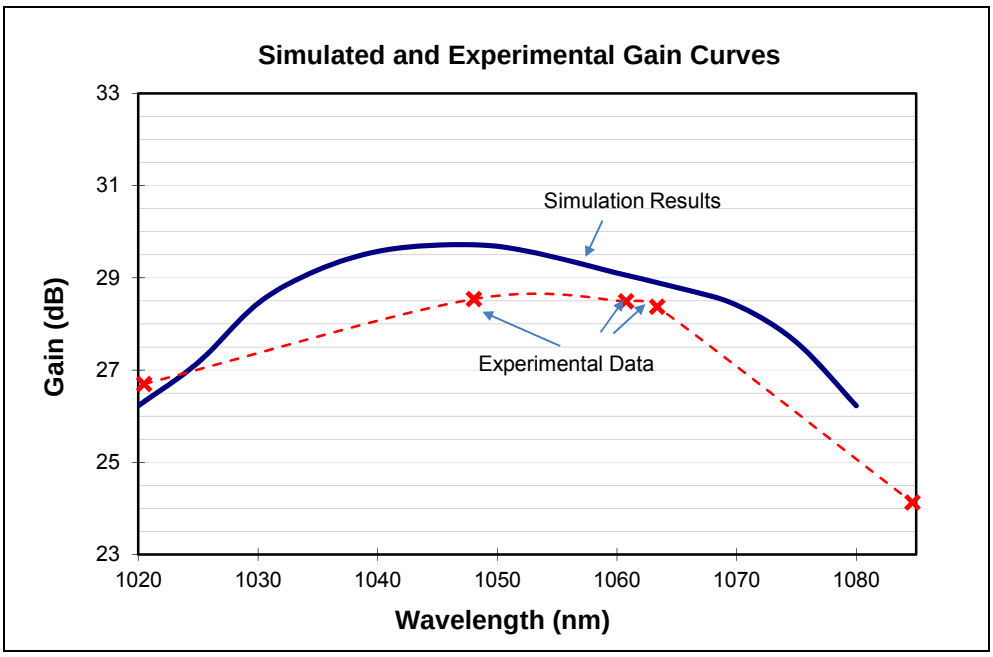

Fig. 15a. Simulated and experimental gain spectra

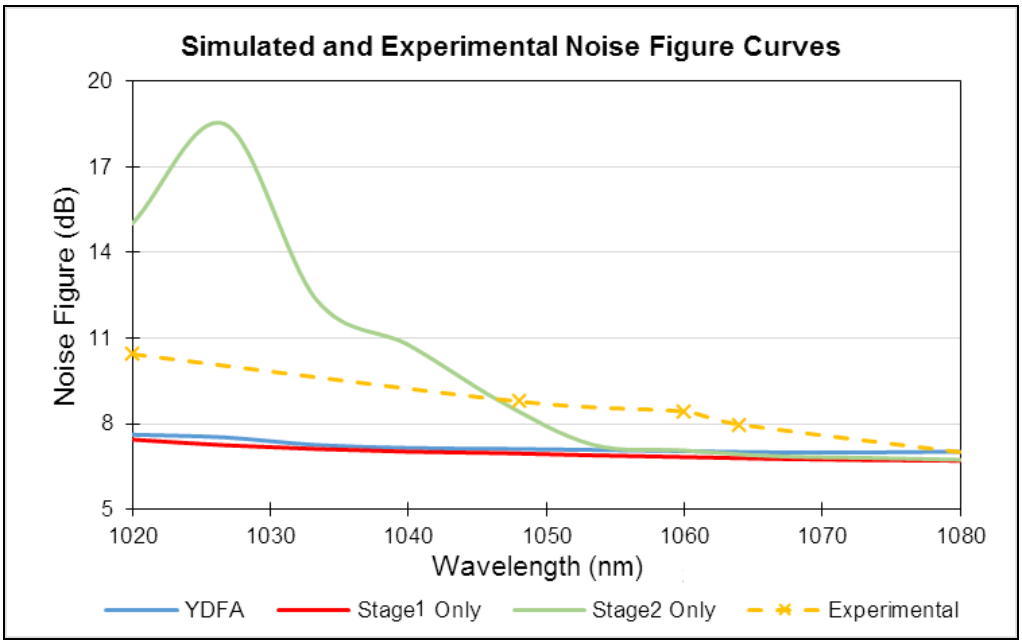

Fig. 15b. Simulated and experimental noise figure spectra

The characteristics of the fiber amplifier noise figure are also studied. Fig. 15b shows the simulated results and the experimental data. The blue line shows the noise figure of the overall fiber amplifier. The red line shows the simulated noise

figure of the stage one amplifier only, which dominates the overall noise figure. The green line is the noise figure of the stage two amplifier only. The noise figure is high at 1030 nm range since it is the signal absorption range with high absorption. The experimental data show that the noise figure is higher than the simulated results at short wavelength. The main is the limited bandwidth of the input isolator. The insertion loss would be about 2-3 dB higher at 1030 nm range. Therefore, the loss of the isolator reduced the input signal and affect the noise figure directly.

The noise figure ranges from 6-10 dB with 0 dBm input. The typical noise figure of a EDFA in 1550 nm range is around 5 dB. The differences are mainly due to the high insertion loss of the input isolator. The insertion loss of 1060 nm isolator is usually higher than 1550 nm isolator since the material used is different. The loss would reduce the input signal and increase the noise figure directly. Fortunately, for applications such as laser marking and sensing, mainly output signal to noise ratio (OSNR) is considered since high OSNR can give high output signal power.

In this section, we proposed and demonstrated a wide operation wavelength range high gain YDFA. A two-stage amplification utilizing both SCF YDF and DCF YDF is deployed. In next section, we are going to use DCF in high power application, especially in pulse application.

2.2 LMA DCF pulse fiber amplifier

DCF is a new technology which can increase the average power, and also the peak power in pulse application. However, nonlinear effects are important factors that prevent the energy scaling from further increasing. Therefore, the basic approach to generate high power femtosecond pulses fiber laser is to avoid nonlinearity.

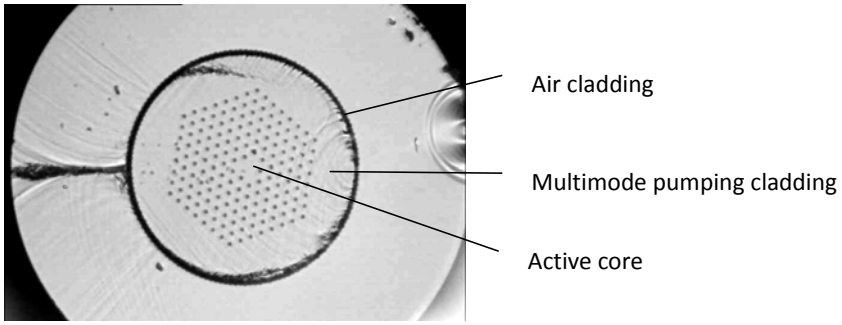

Fig. 16. Microscope picture of the end of PCF fiber (captured from NKT Photonics datasheet).

In order to overcome the restrictions, advanced fiber designs are introduced. Fig. 16 shows the structure of a photonic crystal fiber (PCF) [16]. There is an active core in the middle with several micron diameter and there are many air holes with smaller diameter surrounded. There is multimode pumping cladding and an air cladding.

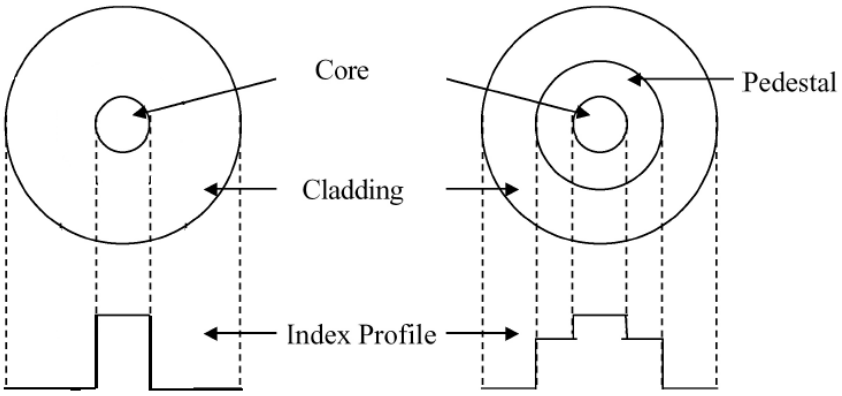

Fig. 17. Schematic of LMA DCF (left), and new type of LMA DCF (right).

However, PCF is not commonly used in the industry when compared to LMA DCF because coupling light to PCF is not easy. It is difficult to splice PCFs with normal fibers. In addition, it is difficult to use conventional high power optical components. On the other hand, use of LMA DCF can achieve high output power level while it can be spliced easily. LMA DCF can also be deployed directly by using a mode field adaptor (MFA). There are two fibers ends of MFA, one is small core and the other one is large core. If both fibers are DCF, we called it a pump pass MFA, which allows both signal and pump lasers to pass through. MFA is built by tapering, which can handle high power.

Fig. 17 shows the schematic of an LMA DCF design. Low core NA can support single mode or few modes. The advanced design can further increase the dopant by pedestal design. The high concentrations of Yb^{3+}, Er^{3+}, and P will increase the refractive index of the base glass, resulting in a relatively high core NA. Pedestal with lower NA can maintain an effective core NA [17].

In this Section, we implement a single mode, linear polarization nanosecond pulsed MOPA fiber laser for LiDAR systems. It consists of two modules, a seed laser and a power amplifier module. It is designed to be cost competitive with other high pulse energy nanosecond laser sources.

High power single frequency fiber lasers with good beam quality can be used in high resolution spectroscopy such as LiDAR. In addition, single frequency lasers with narrow linewidth are often preferred in cases where very small intensity noise is required. Although the gain bandwidth of rare earth doped fiber amplifiers is wide, narrow linewidth seed lasers can still be amplified to high powers with low levels of amplified spontaneous emission (ASE) [18]. Although an LMA fiber core is larger, SBS still limits the power level in narrow linewidth amplification. Also, the fiber length factor cannot be eliminated.

LMA fiber amplifiers can provide good performance not only in single frequency, but also for short pulse amplification [18]. High output power can be obtained by similar configurations. Besides, it can provide a better thermal optical property since the ratio of surface area to volume of fibers is larger which can provide a better heat dissipation performance.

LiDAR system

Solid state lasers are commonly used in coherent LiDAR transmitters. The lasers can provide energy up to milli-Joules and repetition rate about few Hz. High energy is essential for long range detection. However, low repetition rate is not desirable because of possible laser fluctuation and atmospheric conditions from pulse to pulse, which may affect measurement accuracy. Moreover, low repetition rate requires long measurement time. On the contrary, a high repetition rate enables faster measurements. Also, averaging can be used to smooth out speckles and distortions. It also implies that the same pulse energy may not be necessary for LiDAR scan for the same distance range.

As the repetition rate of solid state lasers is confined by thermal problems, we used fiber based systems to improve the limitations, which can provide up to tens of kHz repetition rates. With fiber optic technology, the resulting LiDAR transmitter is compact, small, and light.

As mentioned in the previous Chapter, the fiber based pulse laser is reliable because there is no moving part, and the passive components used can be found in the telecommunication industry. The components are usually able to conform the industrial standard such as Telcordia (Bellcore) testing standard. The life time is long

and the cost is reasonable. Therefore, it is a perfect tool for remote sensing applications, including wind speed measurement, range finding, 3D mapping and hard target characterization.

The designed pulsed MOPA fiber laser source with a few-hundreds of nanoseconds pulses is an optimized design to meet the LiDAR application requirements. If the pulse width is longer, the dead zone of detection is longer for the sensing system. Also, the output transient after amplification would become high for long input pulse width. However, it is difficult for signal detection and signal processing if short pulse width is used.

In addition, AOMs can provide high on-off extinction ratio, which can provide a high resolution for the measuring system. However, AOMs responses are normally several of tens of nanoseconds. Doper effects are the measuring mechanisms and the frequency shift provided by AOMs can allow the wind speed detection in both directions.

In this case, a few-hundreds of nanoseconds can work with pre-shaping in order providing higher output peak power is the most suitable operation configuration. The coming sub-Sections will discuss the detailed system designs and operations.

System design and implementation

Fig. 18 shows a continuous wave single mode 1550 nm laser diode with less than 15 kHz linewidth modulated by a RF driven acoustic optical modulator (AOM) to provide the temporal pulse signal. A preamplifier with polarization maintaining fiber is added in between the seed laser and AOM to boost up the laser power. In order to compensate the AOM insertion loss, a minimum 1 mW of the seed power will be taped out for local oscillator reference.

The seed pulses will go through a high power pulsed fiber amplifier to boost up the pulse energy reaching a minimum pulse energy of 150 μJ at 200 ns pulse width and 10 kHz repetition rate. The pulse will go free space through an optical circulator from port 1 to port 2. The circulator port 2 is terminated with FC/APC connector. The scattered light will be connected and guided to port 3 of the circulator.

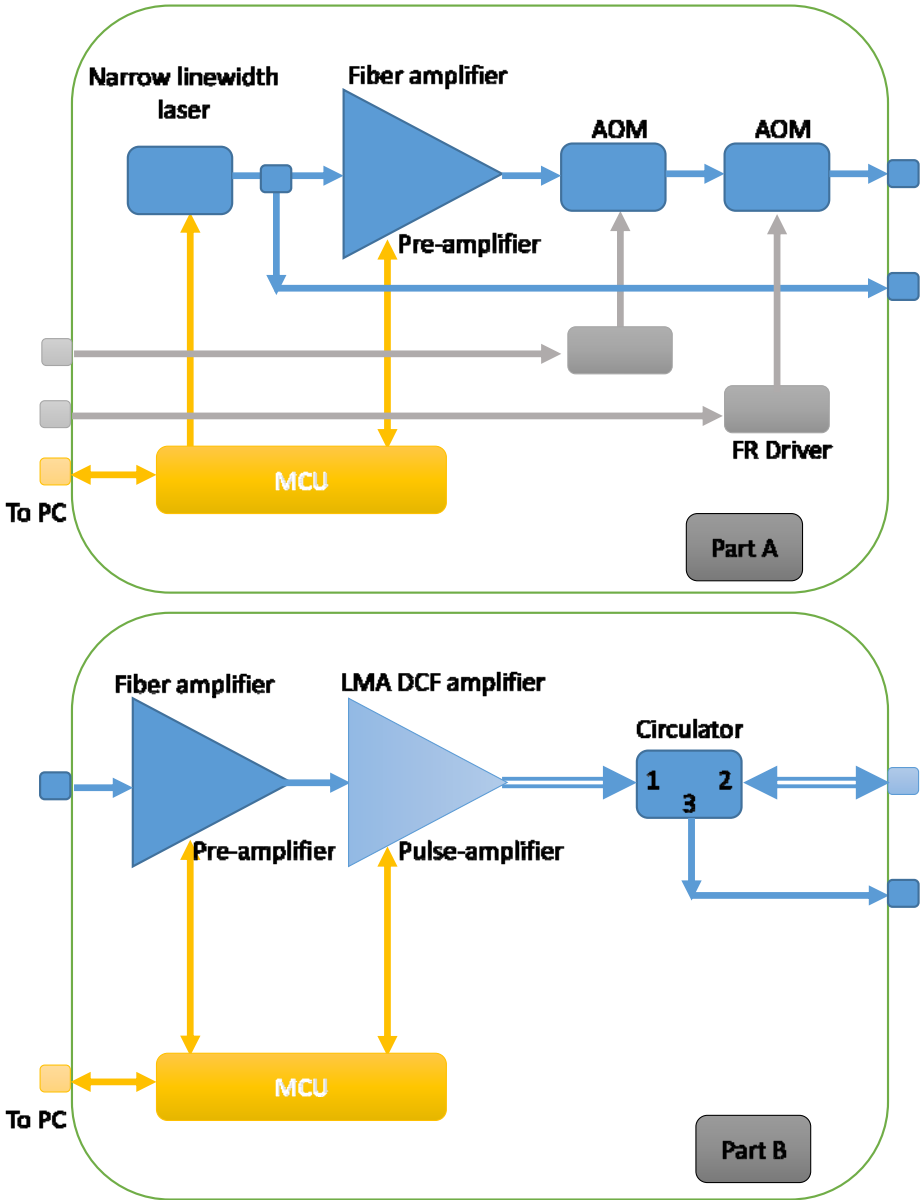

Fig. 18. Schematic block diagram of the fiber laser.

The two modules are housed in an enclosure, which has two layers, the outer layer has cooler and heater in order to maintain the inner chamber temperature in between 10 to 40 degree Celsius. The laser modules need to be mounted on the surface of the inner chamber for heat dissipation. The dimension of the inner chamber is 500 mm x 500 mm x 500 mm.

Two separate modules are used because it allows flexible maintenance or upgrade. Either changing to another seed laser module with narrower linewidth or to another power amplifier module with higher output power can be done separately. There are three key components of the fiber laser including the narrow linewidth laser, the AOM, and the LMA DCF fiber amplifier.

The narrow linewidth laser is the source enabling long distance detection. The AOM provides a frequency shift and pulse generation. The LMA DCF amplifier provides the high pulse energy. In addition, the LMA DCF circulator which captures the back reflection light is also important. The components are developed together with the supplier so that the backward light can be coupled back to normal fiber which can be further amplified easily.

There are two AOMs used. One is analog modulation, and the other one is digital modulation. Besides providing frequency shift and pulse generation, high extinction ratio, and pre-shaping are also given. High extinction ratio increases the resolution of the measurement, and pre-shaping is important to achieve high pulse power with appropriate pulse shape.

Operation and optical performance

Normally, the pulse width required for measurement ranges from 100 ns to 400 ns. If a rectangular shape RF signal is used, a high transient peak is found, which introduces two problems. First, the transient peak power is high enough to trigger non-linear effects such as SBS or damage of the passive components. The other problem is that the FWHM pulse width is too narrow, which cannot be used in LiDAR scan measurement.

In order to achieve a 100 ns symmetry output pulse shape, pre-shaping of the input pulse is needed. Fig. 19a shows the input pulse shape of the RF signal. In this case, a triangular signal is given. The total time duration is 310 ns with 210 ns rise time and 100 ns fall time. A longer rise time and shorter fall time is provided. Fig. 19b shows the output pulse shape with 120 ns pulse width after the AOM. The final output pulse width is 119 ns with pulse energy 106 μJ. All data is measured by an HP83475B Lightwave Communication Analyzer.

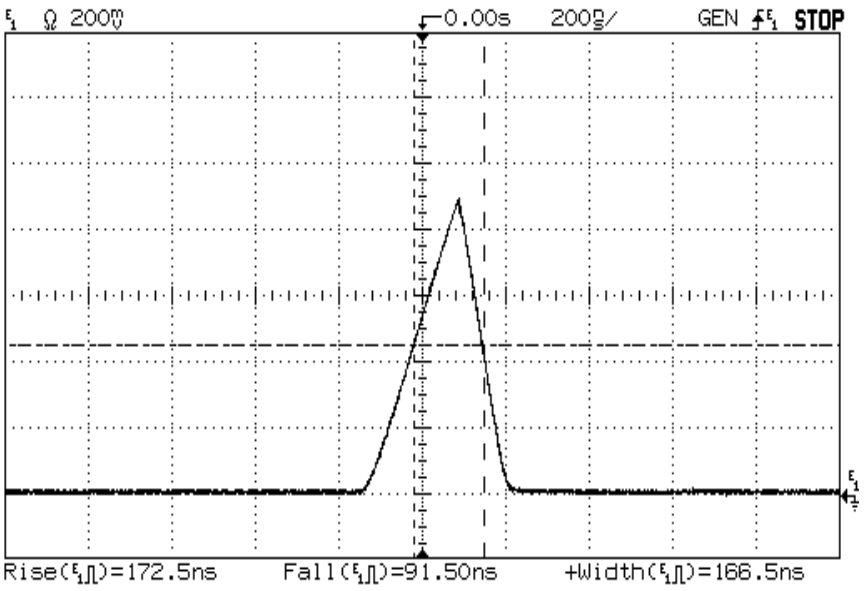

Fig. 19a. The RF input pulse signal in the 100 ns case.

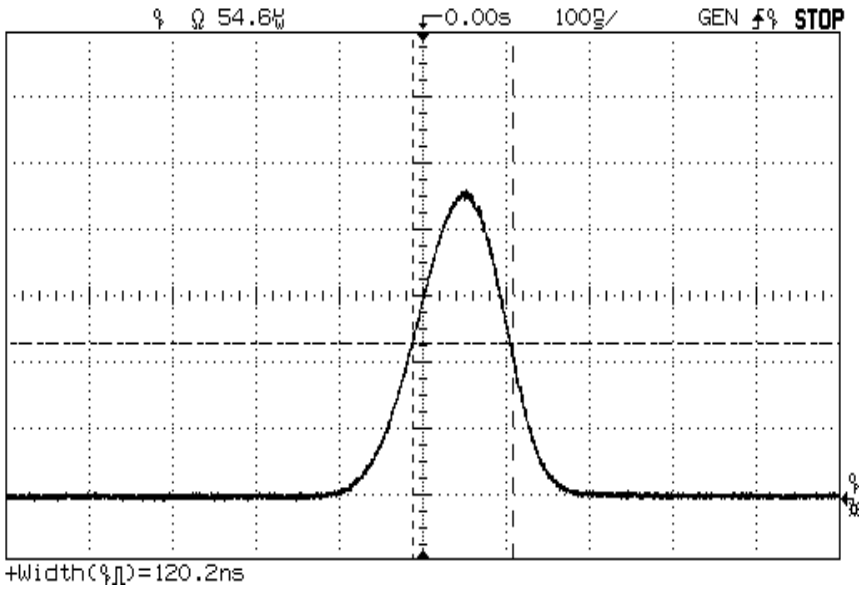

Fig. 19b. Part A output pulse shape in the 100 ns case

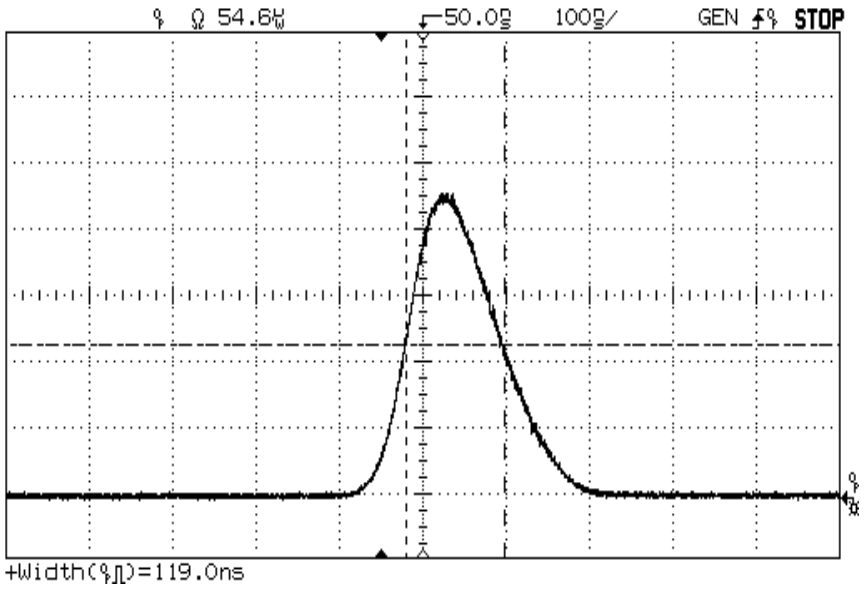

Fig. 19c. The final output pulse shape in the 100 ns case

From the above results, the transient effect during amplification is compensated by the slow rise time pre-shaping in the 100 ns case. To achieve final output pulse with 200 ns pulse width, the pre-shaping RF signal used is shown in Fig. 20a. A triangular signal is given. The total time duration is 570 ns with 470 ns rise time and 100 ns fall time. From Fig. 20b, the output of the AOM shows a triangular like shape with 214 ns pulse width. The shape is a flipped horizontal triangular shape of the input pulse. If we consider the FWHM of the pulse, it is still in the gain transient egion. The output pulse shape is 215 ns, and the pulse energy is 173 μJ.

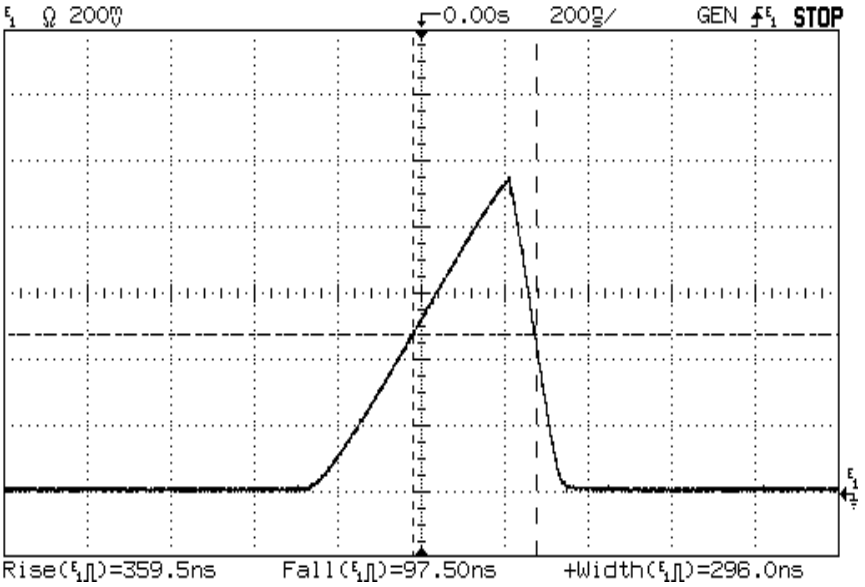

Fig. 20a. The RF input pulse signal in the 200 ns case.

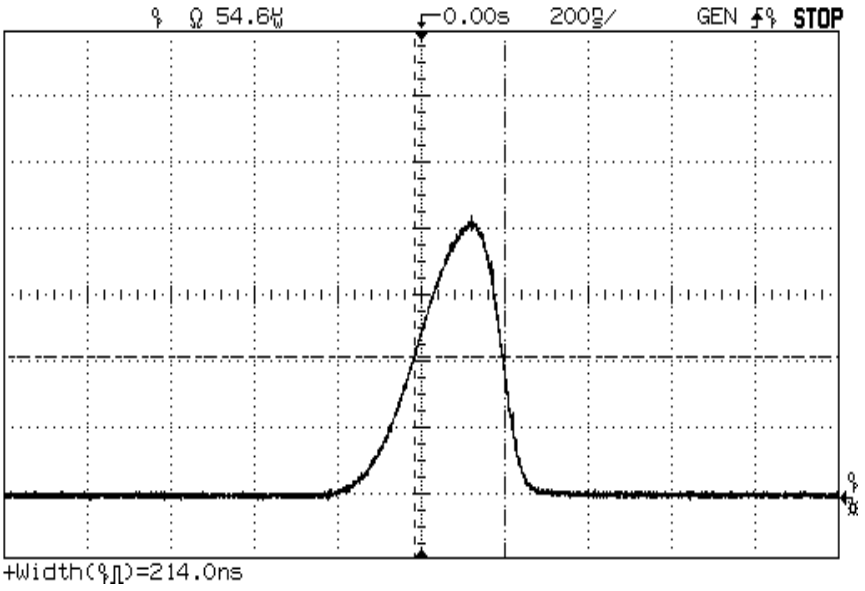

Fig. 20b. Part A output pulse shape in the 200 ns case.

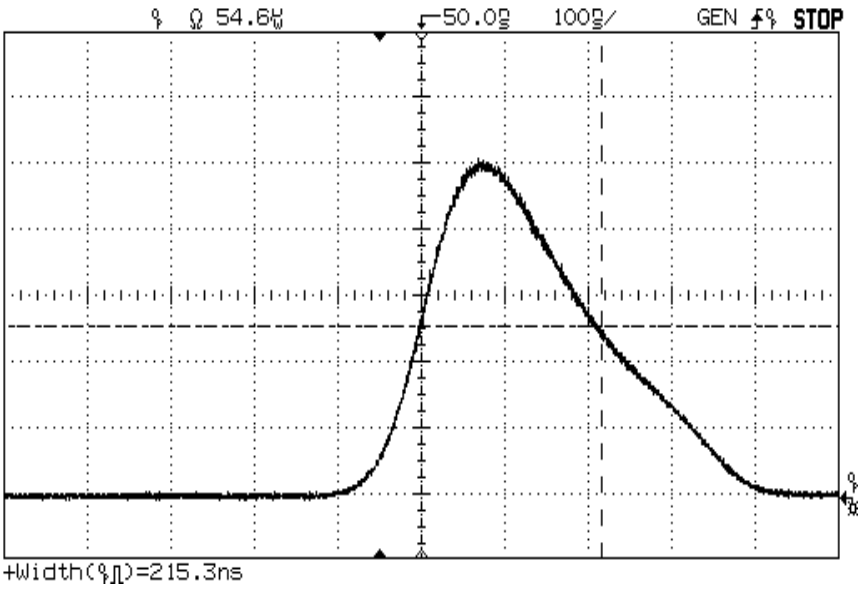

Fig. 20c. The final output pulse shape in the 200 ns case.

To achieve the final output pulse of 400 ns, the pre-shaping RF signal used is shown in Fig. 21a. A triangular signal is obtained. The total time duration is 840 ns with 740 ns rise time and 100 ns fall time. Fig. 21b shows the output of the AOM with 368 ns pulse width. The final output pulse has a 399 ns FWMH width with pulse energy equals 175 μJ.

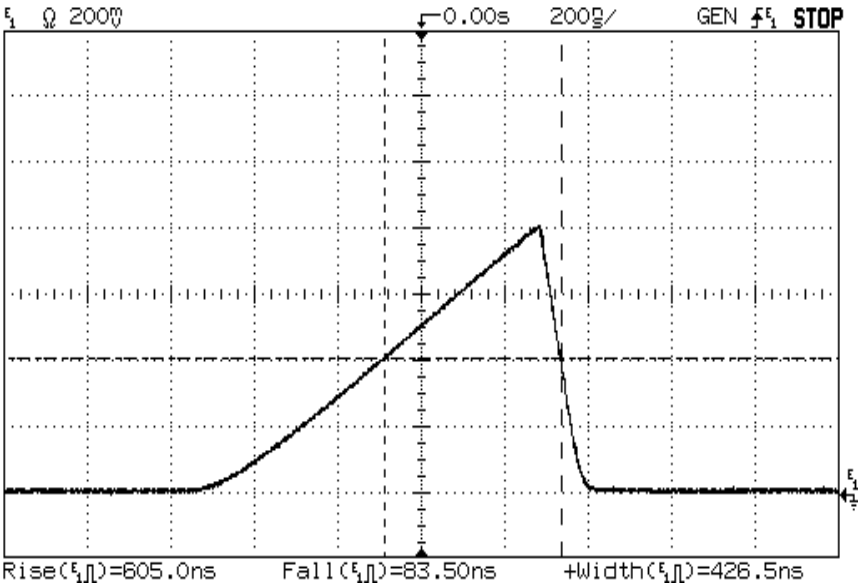

Fig. 21a. The RF input pulse signal in the 400 ns case.

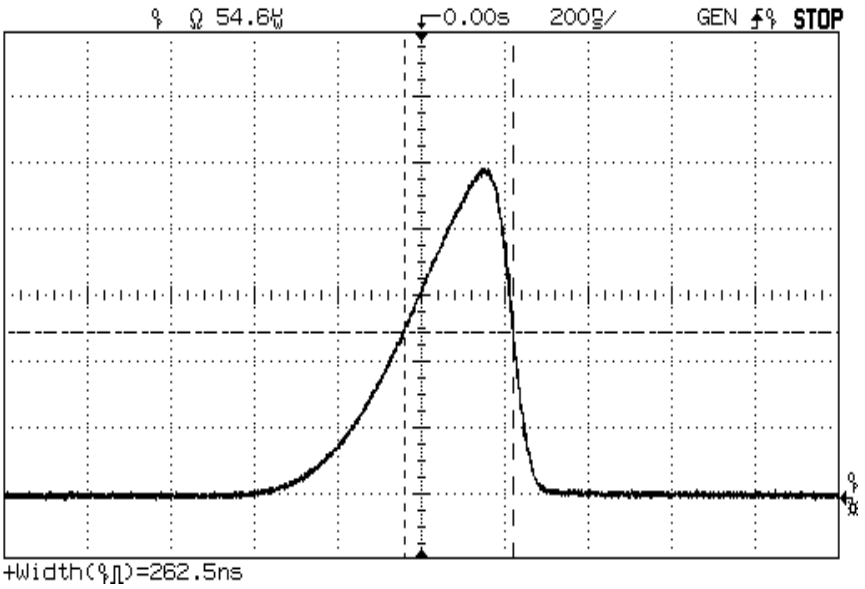

Fig. 21b. Part A output pulse shape in the 400 ns case.

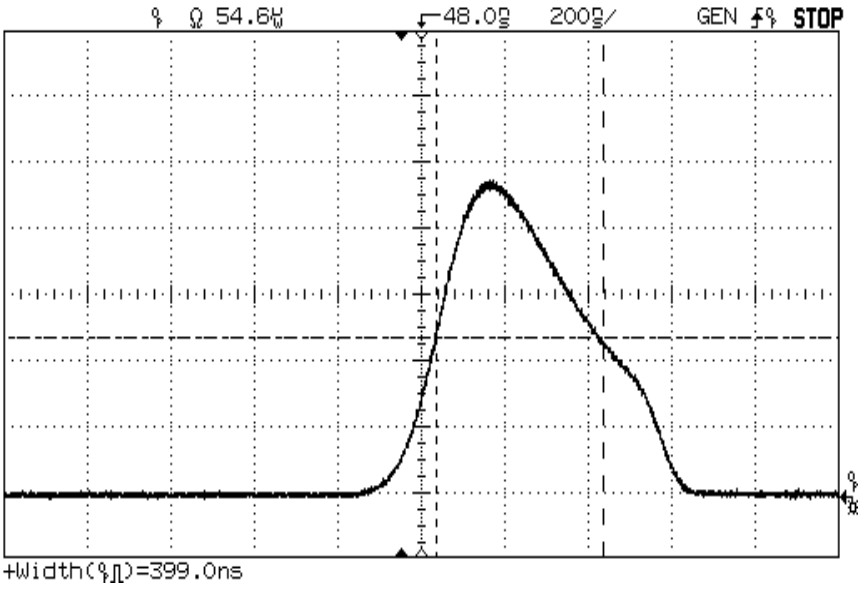

Fig. 21c. The final output pulse shape in the 400 ns case.

Maximum Operating Condition for different pulse width (ns)	*Maximum Operating Current (mA)*	*Maximum Output Pulse Energy (μJ)*
100	3500	106
200	4200	173
400	4200	175

Fig. 22. The maximum output peak power in at pulse width of 100 ns, 200 ns, and 400 ns.

The corresponding results of the amplified output are shown in Fig. 22. Fig. 22 shows the maximum energy with pre-shaping that does not trigger the SBS effect. The corresponding highest operating current in each particular case is also shown. If the current is increased beyond the maximum values, pulse breaking as well as surge of reflected pulses at the circulator due to SBS effect were observed. Fig. 23 - 25 show the measured operating conditions of the laser.

Driving Current for 100 ns pulse (mA)	*Pulse Energy (μJ)*	*Output Power (mW)*
2000	7.1	50
2500	36.9	310
3000	69.8	570
3500	106.9	840

Fig.23. Output power, pulse energy at 100 ns pulse width

Driving Current for 200 ns pulse (mA)	*Pulse Energy (μJ)*	*Output Power (mW)*
2000	8.4	80
2500	40.2	350
3000	80.3	650
3500	114.4	950
4000	156.3	1220
4200	173.6	1380

Fig.24. Output power, pulse energy at 200 ns pulse width.

Driving Current for 400 ns pulse (mA)	*Pulse Energy (μJ)*	*Output Power (mW)*
2000	9.2	70
2500	41.1	350
3000	80.4	640
3500	118.2	940
4000	153.7	1260
4200	175.4	1370

Fig.25. Output power, pulse energy at 400 ns pulse width

It is found that the output power can be varied by changing the pre-shaping RF signal. The digital RF signal is also needed to be customized so that the digital AOM allows the pulse to pass through but cut off the ASE noise in order to increase the extinction ratio. A pulse pattern generator with two channels is used. One channel is used as digital RF input, and the other is used as analog RF signal input. Time delay is needed to compensate the fiber delay, and the difference of response time and the response delay of the AOMs.

Current LiDAR design for wind speed detection is already optimized. There are two trends to further develop the system. One is to increase the pulse energy by using shorter pulse width, such as using SOA to generate the pulse. Use of special fibers to increase the SBS threshold is also being investigated.

The other trend is to change the operating wavelength to 2 μm range. The detection range of LiDAR systems in 2 μm ranges is longer when compared to the 1.55 μm LiDAR systems. Although the components and receivers are expensive in the

2 μm, LiDAR systems at 2 μm perform better not only with longer detection range, but also better detection in bad weather conditions.

Analysis of mode field stripping and beam quality

LMA DCFs are slightly multimode fibers. Techniques such as fiber tapering, fiber bending [20-21] are used to maintain single mode operation. The principle is to increase the loss of higher-order transverse modes. Proper handling of fiber is needed in order to maintain single mode operation in the slightly multimode fiber [22]. The diffraction limited of a step index with mode field diameter (MFD) is up to 30 μm [23].

To demonstrate the effect, a fiber laser with LMA DCF amplifier is built at 1064 nm. It is a PM high power source by using MOPA. The seed laser is a directly modulated pulsed DFB source with 100 kHz repetition rate and pulse width ranging from 10 ns to 1000 ns.

Two beam profiles of the beam exiting the fiber collimator with a repetition rate of 100 kHz and pulse width of 100 ns are measured. Fig. 27a shows the beam profile close to the collimator indicating beam focusing. No lens is used other than the output collimator with a diameter of 150 mm. Fig. 27b shows the beam profile about 45 cm from the collimator. The above beam profile indicates beam divergence and multimode behavior. From these two profiles the beam divergence is estimated to be about 10 mrad.

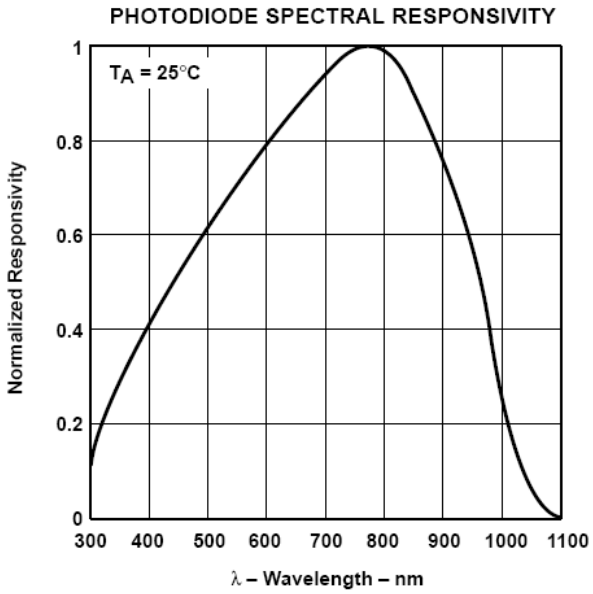

Fig. 26. Typical photodiode responsivity

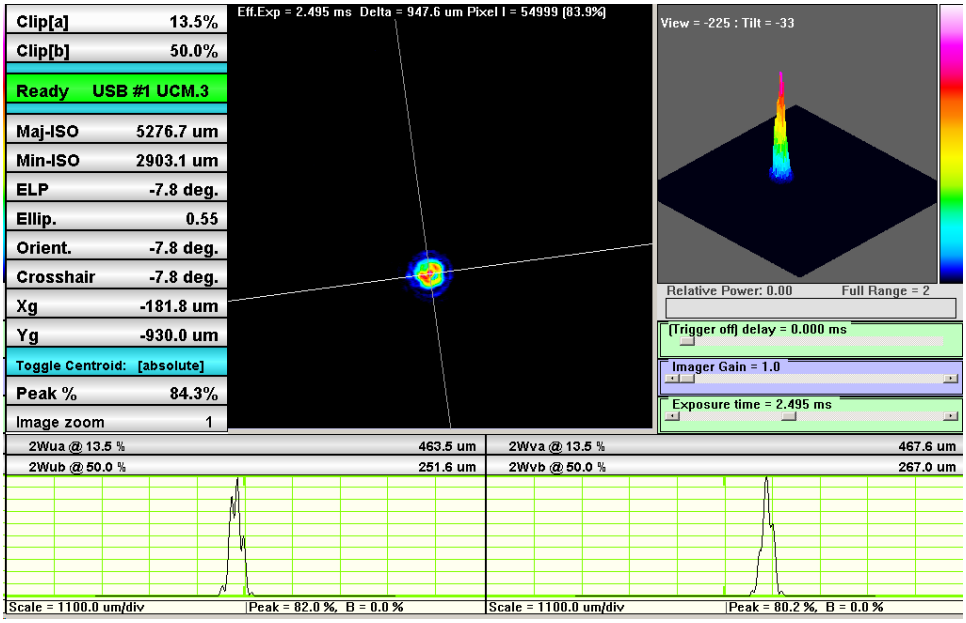

Fig. 27a. The beam profile of pulse repetition rate of 100 kHz and pulse width of 100 ns (from the collimator)

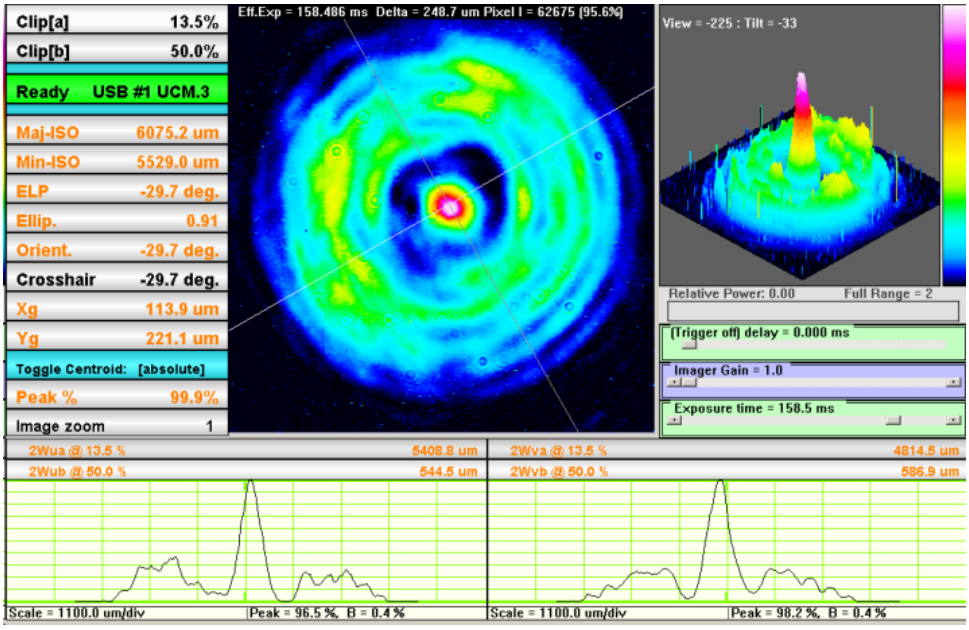

Fig. 27b. The beam profile of pulse repetition rate of 100 kHz and pulse width of 100 ns (45cm from the collimator)

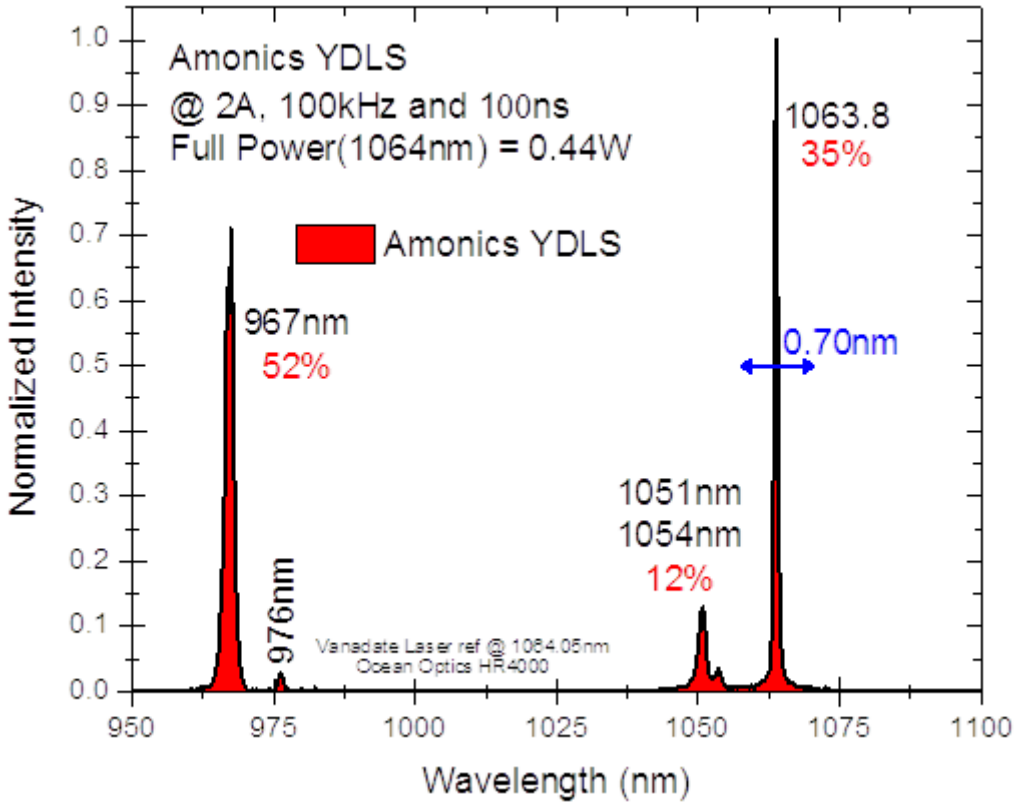

Fig. 28. Output spectrum of the YDLS fiber laser at 100 kHz and 100 ns

Fig. 28 shows three spectral regions at 967, 1051 and 1054, and 1063.8 nm corresponding to significant pump leakage at about 52% of total output power, the cladding ASE at about 12% of the total output power, and the desired lasing transition at about 35% of the total output spectral power respectively. The integrated area of each spectral region was used to determine the percentage of spectral output power and was verified by using a narrow bandpass filter with a measured transmittance at 1064 nm.

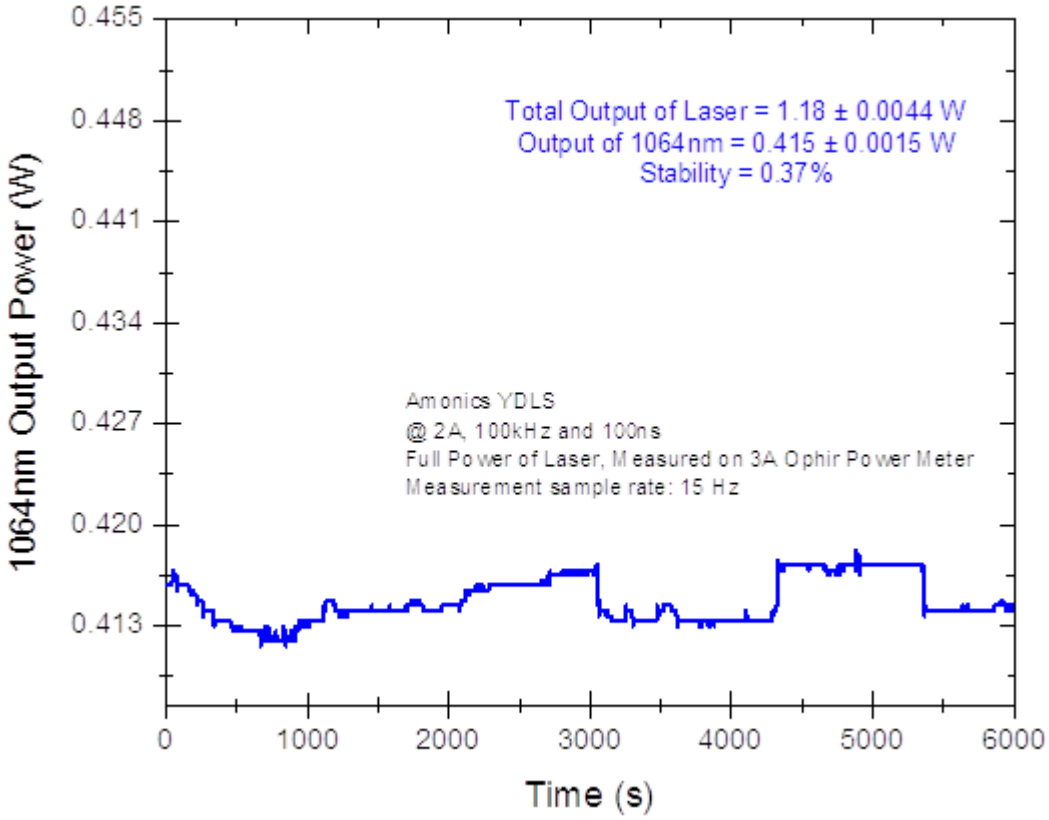

Fig. 29. Output power and energy stability at 100 kHz and 100 ns.

Since there are some pump leakage and cladding 1050 nm ASE, the power at

1064 nm was determined by two different methods. The first method is accomplished by using the spectral strength of each wavelength region shown in Fig. 28 for the percentages of pump, glass self lasing, and 1064 nm. Since the stability of each of these wavelength bands is high, this is a fairly accurate method to determine the output at a particular wavelength. At the above pulse repetition frequency and pulse width, the energy at 1064 nm is 60% of the total energy. Also, the energy stability at 1064 nm, determined by the standard deviation of energy readings, is also proportional to the total output energy. The second method to determine the output at 1064 nm used a calibrated narrow band filter at 1064 nm. All other wavelengths are blocked by an optical densities (OD) short pass filter. Both methods to determine the energy at 1064 nm agree to within 1%. Since the repetition rate, 100 kHz, is too large for most energy meters, a power meter was used.

Fig. 29 shows that the laser can be stable for 1 hour 40 min. Fig. 30 shows the temporal profile of the trigger RF input signal and the corresponding output at 1064 nm. Fig. 29 also shows significant modulation with very little pulse to pulse instability. Three traces taken five minutes apart are superimposed over the red curve showing a stable modulated pulse output. The input RF pulse set to 100 ns triggered a pulse of 86 ns at full width at 1/e max (FW1/eM).

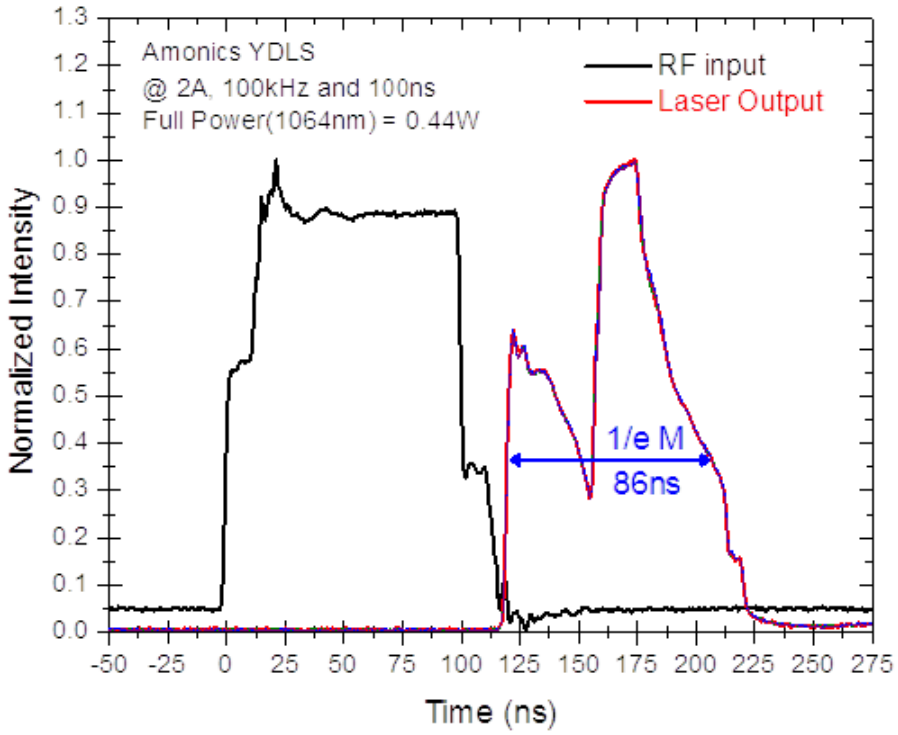

Fig. 30. Temporal profile of triggered RF input signal and the corresponding 1064 nm laser output

The wavelength separation was obtained by using dielectric mirrors which passes the desired wavelength and reflects any wavelength outside the range. It is found that the total output shown in Fig. 31 does not very modulated significantly since the silicon detector used has a much larger responsivity at 967 nm than at 1064 nm as shown in Fig. 26. Responsivity at 967 nm is about five times higher than that at 1064 nm.

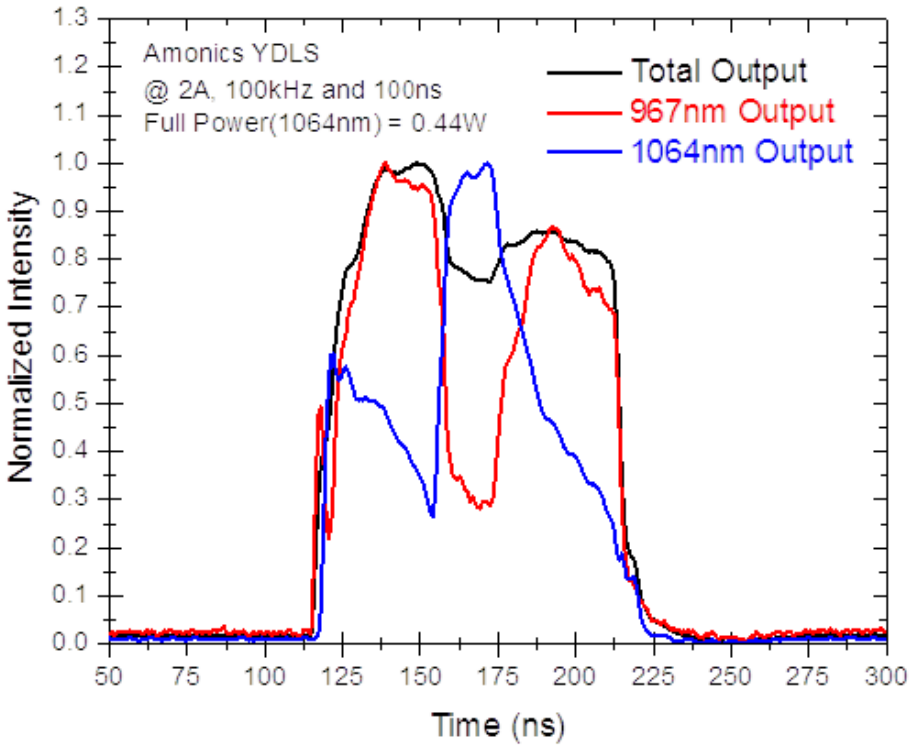

Fig. 31. Normalized temporal output of total, 967 nm, and 1064 nm shown in black, red, and blue, respectively at 100 kHz and 100 ns.

Improvement of the laser design

It is found that the laser source is stable. The main problems are the cladding light, including both the residual pump and the 1050 nm ASE. In addition, two peaks are found, which is due to the tuning of the directly modulated DFB. In order to remove the signals, we need to guide the signals out from the fiber cladding. Originally, we used a pump dump. Pump dump is a device guiding the cladding signals out from the fiber. First, the fiber coating is stripped by using a fiber heat stripping. Then, high index gel is placed on the surface of the fiber. Normally, high index larger than 1.5 ultraviolet (UV) glue is used, and the pump dump is located at the splicing point. The fiber is located on a metal panel with a groove, and then UV

curing is carried out to fix the position.

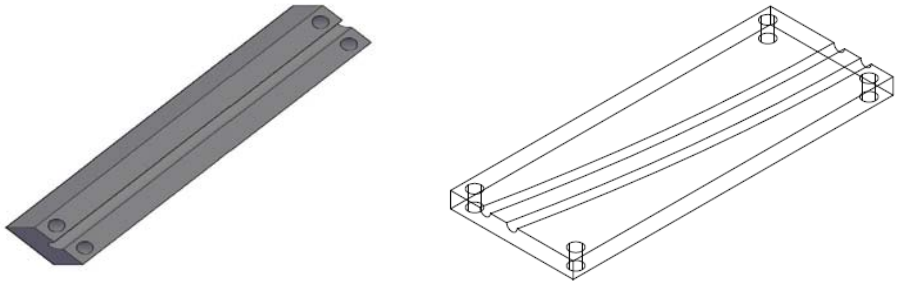

Fig.32 Original pump dump design (Left) and new pump dump design (Right)

It is found that the pump dump is about 93-94% only for the original pump dump design. Since the total pump is about 16 W, and the total absorption is about 18-19 dB, the pump leakage can be up to several hundreds of milliwatts. In fact, the pump absorption should be more than 22 dB at 976 nm, however, the wavelength cannot be locked properly by the volume Bragg gratings (VBG) within the multimode laser diodes due to the low driving current. The problem with the residual cladding pump would worse if the pump power is higher. Therefore, three processes are needed. The first is to use a 976 nm multimode laser with lower rating and lower locking power. The second one is to improve the pump dump method. Finally, we need to modify the direct modulation circuit of the DFB.

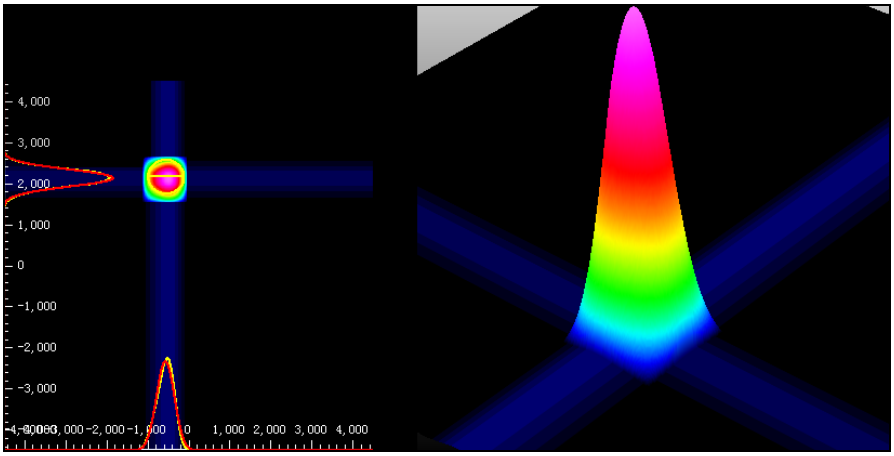

Fig. 33. Beam profile after rework (45cm from the collimator).

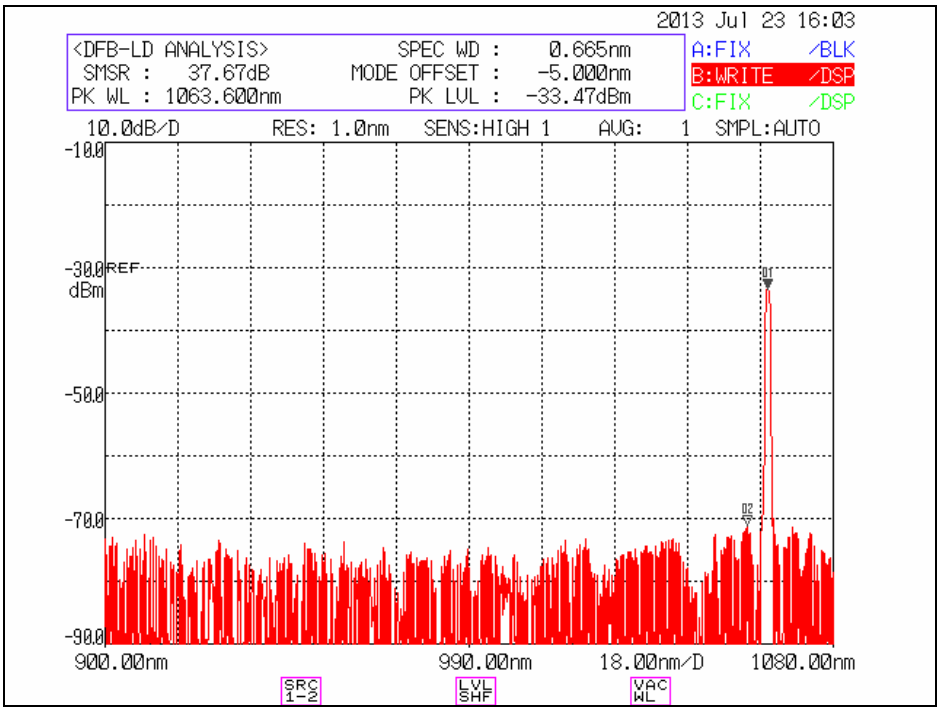

Fig. 34. Output spectrum of YDLS fiber laser after rework.

We changed the design of pump dump. Fig. 32 shows the original and the new designs. There are two pump dump areas with some bending in the new design. As a result, more than 99% residual pump can be dumped. A free space photo detector is used to capture the light coming out the pump dumps. The beam profile and the spectrum from the collimator output are also captured.

Fig. 33 shows the beam profile after rework 45 cm from the collimator. Fig. 34 shows the output spectrum of the YDLS fiber laser. There is no output power other than the 1064 nm measured.

2.3 Conclusion

A number of new technical improvement are needed when building DCF and LMA DCF lasers and amplifiers. Fiber length is one of important design parameters. Then, if it is important to consider the operating wavelength range, SBS and SRS, pulse shape in pulse application, signal power, non-linear effect, etc.

The effect of using different pump lasers, such as 915 nm, 940 nm, and 976 nm VBG multimode pump lasers, are studied. We selected the pump by considering the absorption effect, and the effect of pump wavelength shifts due to temperature variation. Discussions with pump laser manufacturer on how to improve the heat dissipation and how to improve the welding skill were carried out. In addition, the number of pump diodes used, the corresponding power rating, and the appropriate pump combiner are also considered.

For LMA DCFs, two designs of using combiners are studied. One is to use an MFA to convert the signal from normal fiber to LMA fiber and use a LMA combiner for further amplification. The other one is to use a normal combiner to combine the pump and signal and then use an MFA with pump pass for further amplification. The main consideration is the mode quality and the stability of the laser output.

Some of the experiments, such as improving the beam quality are carried out together with the manufacturer. The construction and limitation on pump pass and

non-pump pass MFA are also discussed. For example, backward pumping for pulse amplifier can use shorter fiber and the non-linear threshold will therefore be higher. However, the output beam quality from the LMA combiner is not as good as a normal combiner. In addition, splicing of LMA fiber is difficult and long fiber is needed which can reduce the non-linear threshold as a result.

Recoating are needed after splicing DCF fiber to DCF fiber in order to allow pump light to pass through. Low index polymer is used because the low reflective index will keep the pump power within the inner cladding. Same as normal DCF, low index polymer is used for the recoating LMA DCF. Since recoating of LMA DCF is needed, optimization of the curing process is carried out by using different ultraviolet (UV) light exposure intervals and UV light intensity. It is suggested that the minimum UV dosage for complete cure is 1000 mJ/cm^2 in nitrogen environment. However, the UV dosage is heavily dependent upon the thickness of the polymer layer and the drawing speed.

When there is residual pump at the end of the active fiber, we need to remove the pump from the cladding. Otherwise, the passive components after the active fiber, such as the isolator, would be damaged. Normal pump dump by using high index jam can only remove about 93-94% of the residual pump. Longer pump dump can increase the factor up to about 97%. If two pump dumps are considered, the

factor would be up to 98%. Two pump dumps with additional bending in between can provide a factor larger than 99%.

Cladding signal means the signal light prorogates through the inner cladding instead of the core. Besides residual pump, cladding signal would appear after amplification. The beam quality would therefore be affected. By using two pump dumps with additional bending in between can remove the cladding signal and improve the beam profile.

Since high average power or peak power is considered, the splicing point cannot withstand the high power if the splicing loss is high. Also, the heat generated by the splicing loss, components, and also the fiber surface are handled carefully, otherwise, the optical performance would not be stable.

In conclusion, by optimizing the optical configuration, especially the fiber length, the method of building fiber lasers or fiber amplifiers with wide bandwidth, low gain variation, high pulse peak power without SBS, narrow linewidth with high extinction ratio are studied.

Chapter 3 Mode-locked fiber lasers

In general, lasers can run in continuous wave (CW) or pulse mode. Different from CW lasers, the peak power in pulse lasers is higher. The high pulse energy can be used in applications, including material processing, such as cutting, marking, and drilling holes. In addition, pulse lasers can also be used in imaging, microscopy, spectroscopy, and remote sensing.

Mode-locked fiber lasers are commonly used because of the high gain efficiency of active fibers. Relatively low pump power can be used in the laser cavity together with optical filters, isolator, polarization controller, and even dispersion compensation fiber, which could not be used in bulk lasers. Mode-locked fiber lasers are compact and robust.

Most of the optical components needed to build mode-locked fiber lasers, such as rare earth doped fibers, isolators, and optical filters are commonly used in telecommunication. The components used are the same used to build optical amplifiers. The cost is reasonable, and compatible with telecommunication systems.

3.1 Principle of mode-locking

There are many longitudinal modes in a simple laser. Each individual longitudinal mode has finite bandwidth which is determined by the cavity Q factor. In general, there is not any relationship among them. It is equivalent to many independent lasers with slightly different frequencies co-existing in the cavity. In addition, the phase of individual longitudinal mode may vary randomly. Thus, constant output intensity can be obtained when there are thousands of modes. However, if interference between different modes occurs, the output intensity fluctuates.

When a laser is mode-locked, each mode operates with a fixed phase difference. Constructive interference happens among these modes will then result in a pulse of light. If there is only one pulse in each round trip time, the interval between each pulse is

$$\tau = 2L/c, \tag{13}$$

where τ is trip of the laser cavity, L is the cavity length, and c is the light speed. If a ring cavity is considered, the multiplier two in the right hand side of Eq. (13) becomes one. Thus, the mode spacing of the laser is

$$\Delta\nu = 1/\tau. \tag{14}$$

Normally, a laser cavity is several meter to tens of meter long. From Eqt. (13)

and (14), the mode spacing is about several MHz. If the laser linewidth is 50 GHz (about 0.4 nm in 1550 nm range), there are already more than thousands of modes within a laser cavity. The method of reducing the number of modes has been discussed in Chapter one.

There are two main methods to achieve mode-locking, namely active and passive mode-locking. An external RF signal is used to induce modulation in active mode-locking. Passive mode-locking uses a non-linear component such as saturable absorber to generate self-start modulation.

The pulse width is determined by the number of cavity modes in phase. The mode-locked bandwidth, B_{lock}, is $N\Delta\nu$, where N is number of locked modes and $\Delta\nu$ is the frequency separation. The bandwidth is inversely proportional to the pulse width. The pulse width is determined by the pulse shape. The amplitude and phase relationship of each longitudinal mode is required. The minimum possible pulse width, Δt, provided by a laser with a Gaussian temporal shape is

$$\Delta t = 0.441/ B_{lock} . \qquad (15)$$

The time-bandwidth product is pulse shape dependent. For a pulse with Gaussian shape, the time-bandwidth product is 0.441. For a hyperbolic secant squared pulse, which is commonly used in ultrashort pulse, the corresponding time-bandwidth product is 0.315.

The minimum pulse width can be calculated from Eq. (15). For example, if the laser with a 50 GHz spectral width, the shortest pulse width is about 100 fs. In general, the pulse widths of mode-locked lasers depend on the pulse shape and pulse chirp.

For a given spectrum, the minimum pulse width is obtained in a transform-limited pulse. In a transform-limited pulse, the time bandwidth product is at its minimum and there is no chirp. For a given pulse width, the spectral width is at the minimum for transform limited pulses. This is important in optical fiber communications. The transmission length can be increased if the signal is close to transform limited pulses. The effect of chromatic dispersion in fiber will then be minimized. Soliton laser is a pulse laser that able to generate close to transform limited pulses.

Active mode-locking

In general, an optical modulator is used in active mode-locking. An optical modulator provided with a sinusoidal signal can produce amplitude modulation of the light in the cavity. For example, if optical signal frequency is ν and the modulation frequency is f, then two optical sidebands frequencies ν − f and ν + f are generated. If the cavity mode space Δν matches the frequency f, these sidebands would be equal to the two cavity modes. The main mode and the two cavity modes will then be in phase, and locked together. Afterwards, ν − 2f and ν + 2f modes and all cavity modes are locked. Another active mode-locking method is synchronous pumping. The working principle is similar, locking the cavity mode by providing a pump modulation frequency.

Passive mode-locking

Different from active mode-locking, external RF signal is not required. Non-linear devices such as a saturable absorber is used in passive mode-locking. It is an intensity dependent transmitter. The loss of the device depends on the input light intensity. In other words, a saturable absorber in passive mode-locking will amplify and transmit high intensity light only. After a number of round trips in the laser

system, a pulse train is formed.

In a passively mode-locked laser, the response time of the saturable absorber is one of the factors determines the final pulses width.

Methods of passive mode-locking

Semiconductor saturable absorber mirrors (SESAMs) and carbon nanotubes (CNTs) are commonly used in passive mode-locking. SESAM is a mirror structure with saturable absorption. Stable passive mode-locking with self-starting [24] can be achieved by using SESAM.

CNT can also be used in mode-locking with loss at about 0.3 dB [23]. Different from SESAM, CNT can be used in transmit type. It can be used in either linear configuration or ring configuration. The first CNT mode-locked fiber laser is a ring laser [23]. In our experimental setup, it is found that CNT can self-start passive mode-locking and operate in single pulse region.

Lately graphene attracts much attention because of its unique electronic properties. Compared to traditional SESAMs, the major advantage of graphene is the intrinsic wide-band operation. Graphene has lower loss and higher damage threshold [26] when compared to CNT. However, graphene is still in research stage and no commercial product is available in the market. Therefore, the system is not reliable

when compared to SESAM and CNT.

Figure-eight configuration is another passive mode-locking scheme. Non-linear optical effects in the laser cavity are able to provide selective amplification of high intensity light. It will be further discussed in next Section.

Improved stability of passive mode-lock lasers

Since the repetition rate of passive mode-locked lasers depends on the laser cavity, the frequency will drift when the fiber temperature changes. In order to achieve better frequency stability, the temperature of the fiber is maintained at a temperature controlled chamber and there is a fiber module with piezo-electric actuator to change the fiber length.

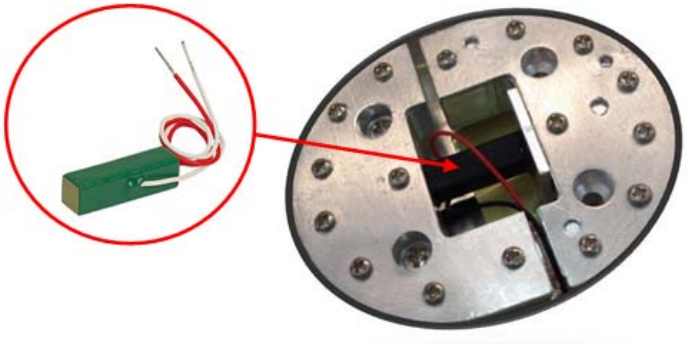

Fig. 36 Left: Piezo-electric actuator (6.5 mm x 6.5 mm x 20 mm); Right: Piezo-electric actuator with fiber module

The dimension of the piezo-electric actuator is 6.5 mm x 6.5 mm x 20 mm. When we applied voltage from 0 to 5 V to the piezo-electric driver, the corresponding output voltage would be ranging from 0 to 150 V. The maximum elongation of piezo-electric actuator is 17.4 μm. Since the fiber length of the module is 185 mm for each loop, the maximum fiber length elongation of the module is 34.8 μm for each loop.

In our experimental setup, we built a passive mode-locked laser with SESAM, and there are 15 fiber loops inside the module. As a result, the maximum elongation

is equal to 522 μm. The total cavity length of the fiber laser is 8 m. The repetition rate from Eq. (13) is,

$$f = c/nL = 25 \text{ MHz, and } \Delta f \sim 1.63 \text{ kHz.}$$

The frequency is 25 MHz and the tunable range is about 1.63 kHz. Fig. 37 shows the control diagram of the passive mode-locked laser. The control circuit read the frequency from the photodiode and compares to the external RF signal. Then, two control signals will be sent to the external actuator, the temperature chamber (TEC) and piezo-electric actuator (PZT).

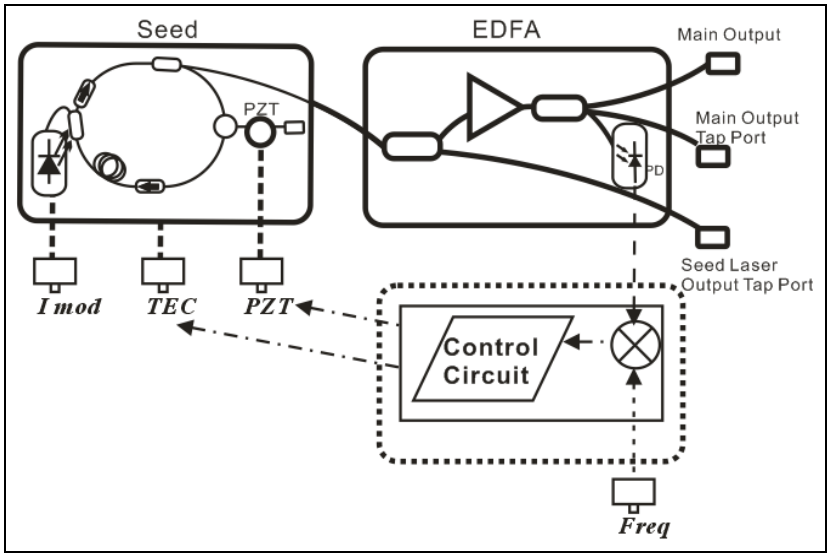

Fig.37. Control diagram of the passive mode-locked laser

The response of the TEC is slow but the tuning range is high. On the other hand, the response of the PZT is fast, but the tuning range is low. The passive mode-locked laser is then integrated to an optical amplifier in order to adjust the pulse power and the optical spectrum range. Fig. 38 shows the measured tuning range. Fig. 39 shows

the repetition rate measured. The output is stable up to Hz variation.

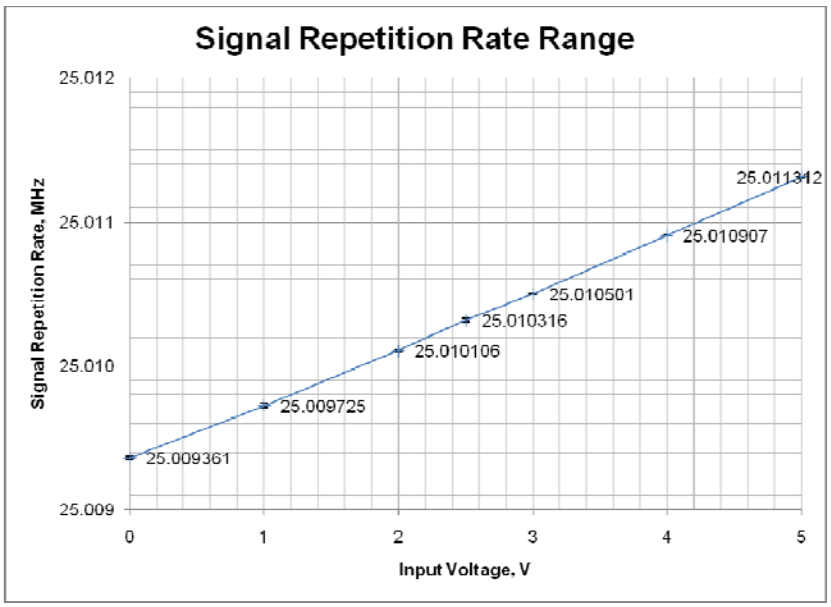

Fig. 38. The tuning range of the repetition rate of the mode-locked laser by using the PZT

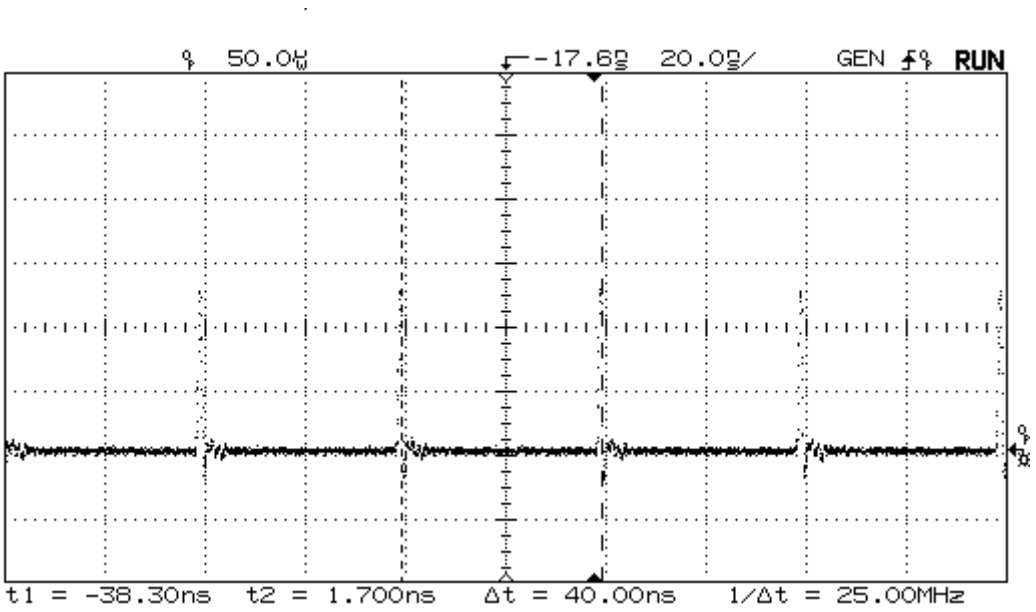

Fig. 39a. Laser output measured by the photodetector

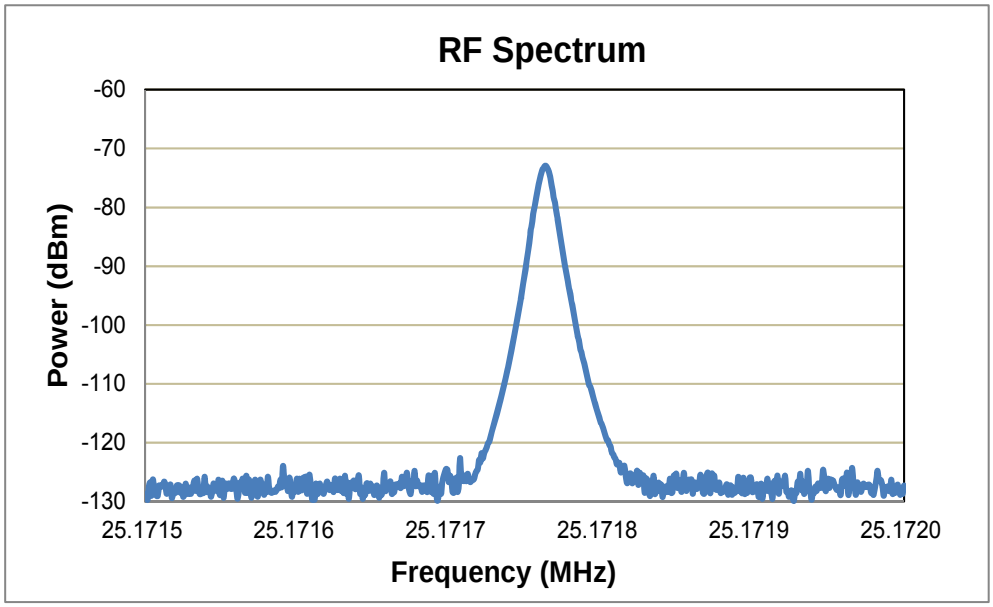

Fig. 39b. The corresponding RF spectrum of the laser output

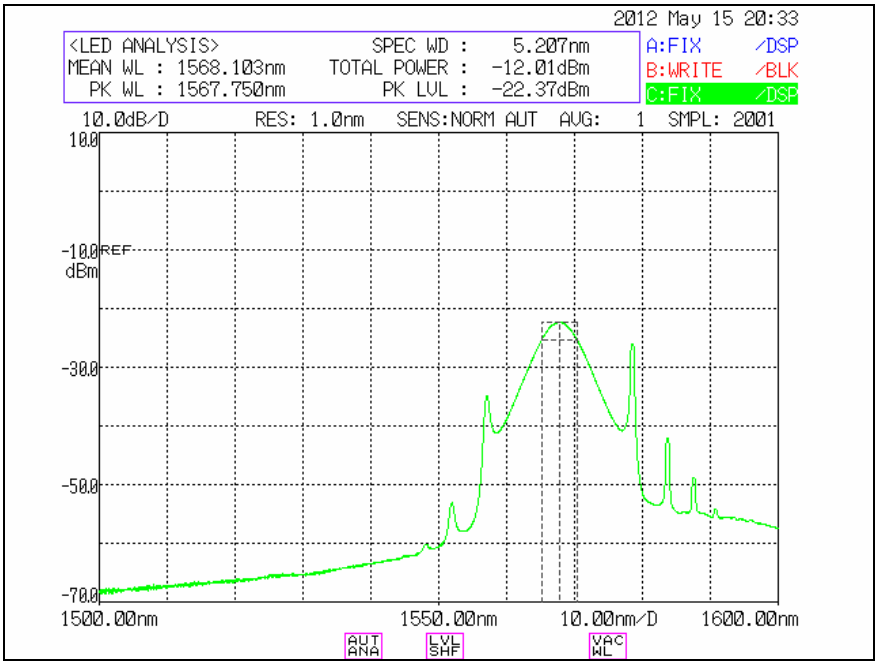

Fig. 40a. The optical spectrum of the seed laser measured from the tap port

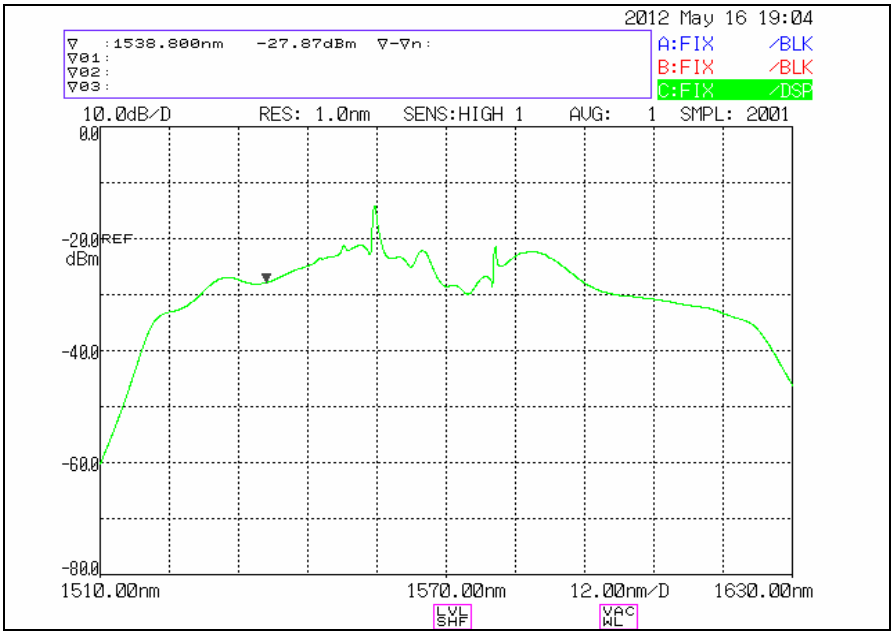

Fig. 40b. The optical spectrum of the output laser

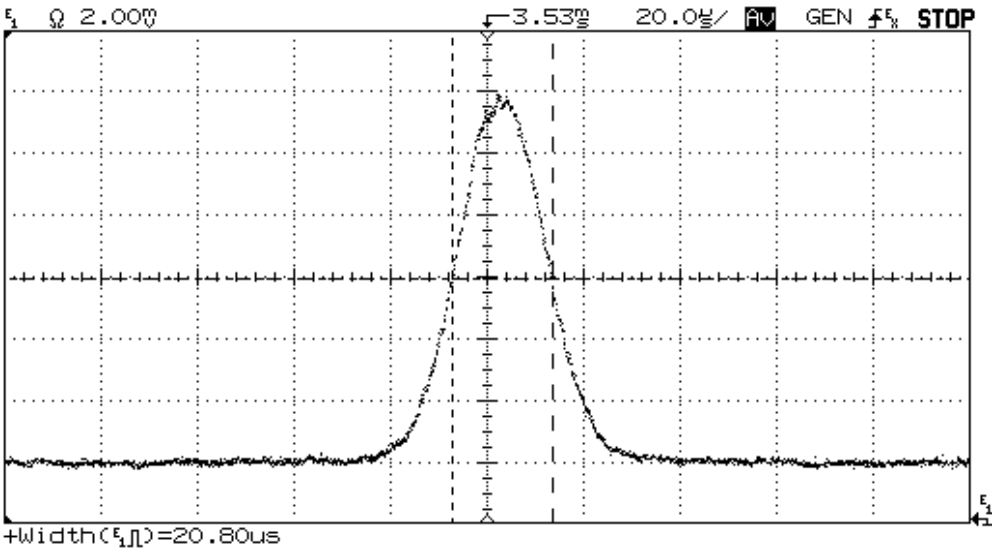

Fig. 41a. Seed auto-correction trace

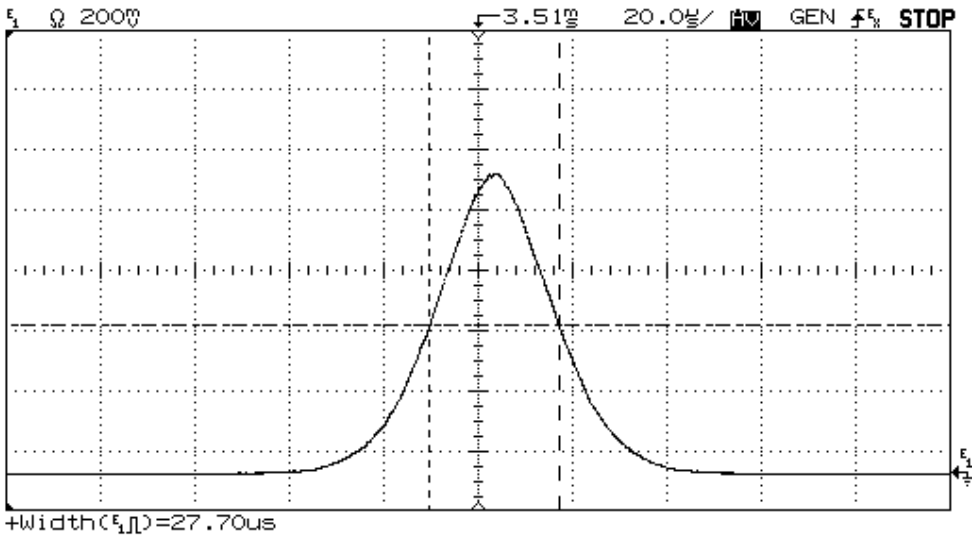

Fig. 41b. Output auto-correction trace

Fig. 40 shows the seed laser spectrum and the output spectrum. The seed spectrum obtained is a soliton, and the corresponding 3 dB spectral width is about 5 nm. An optical supercontinuum spectrum is obtained at output port. The 20 dB spectral wide is more than 100 nm. Fig. 41 shows the auto-correlation traces of the seed laser and the output laser. From the traces, the seed laser pulse width is 432 fs, and the output pulse width is 575.3 fs. The average output power is 13 dBm.

3.2 Ring resonator passive mode-locking

As mentioned in Chapter 2, ultra-short pulse is a popular topic in the study of fiber lasers. 2 μm fiber pulse lasers can be used in applications including sensing, time-resolved spectroscopy, medicine, and material processing. These lasers also find applications in the environmental field because of their unique attributes of being eye-safe and strong absorption by atmospheric gases and water vapor in this wavelength range. They are used in LIDAR (Light Detection And Ranging) to detect wind velocity and track storm.

Tm-doped fiber lasers can cover the 2 μm region from 1.8 μm to 2.1 μm, depending on whether an optical filter is implemented. 2 μm mode-locked lasers can be constructed by using carbon nanotubes, SESAM, nonlinear polarization rotation, or a combination of SESAM and non-linear loop mirror (NOLM). We developed an all fiber mode-locked laser in the figure-eight configuration consisting two coupled loops. By using figure-eight configuration [31, 35], no saturable absorber or other non-linear device is needed. In addition, a figure-eight mode-locked fiber laser can be used as a master oscillator which can provide high average output power, or a Master Oscillator Power Amplifier (MOPA) which can be used in external fiber amplification. The output power of the oscillator is limited by optical elements such as the isolator,

fused coupler, bandpass filter, and the ring resonator which can be up to several hundred mW higher than SESAM. The loss is lower than carbon nanotube.

In this work, we use an 11-th order microring resonator filter to achieve mode-locking in a figure-eight fiber laser. Previously, we reported stable mode-locked pulses in the 1.55 μm range based on Filter-Driven Four-Wave-Mixing (FD-FWM) [29]. Here, the same high-order microring resonator is used to generate optical pulse train in the 1.81 μm range. The present work studied the figure-eight configuration and the ring resonator mechanism.

Background Theory

Previously, a ring resonator was used to generate a stable mode-locked laser at 1.55 μm by FD-FWM [31]. However, because the zero dispersion point of the filter is in the 1.55 μm range and the filter at 2 μm is well into the normal dispersion region, the filter alone cannot provide sufficient FWM to generate stable mode-locked pulses at around the 2 μm range. Thus we proposed to utilize the figure-eight configuration for the laser and an 11-th order filter to achieve mode-locking at around 2 μm.

The wavelength selection is implemented by a wide band filter and the ring resonator. The tunable filter is a wide band 5 nm Gaussian filter with 10 nm tuning range. The ring resonator acts as a narrow band filter, the band width is about 0.6 nm.

Fig. 45 shows the transfer spectrum of the ring resonator. High FSR, about 637 GHz, and high extinction ratio larger than 30 dB can be achieved. The center wavelength can be tuned by tuning the wide band tunable filter to the discrete band. In fact, the center wavelength can be fine-tuned by changing the ring resonator temperature. By using such filter combination, the pulse width would be limited to tens to hundreds of picoseconds. In addition, it helps to achieve stable mode-locking since the number of modes is reduced. The performance of Tm-doped fiber lasers will further be improved only when optical components in 2 μm components are developed.

Fig. 42a shows the schematic of a passively mode-locked optical fiber laser using the figure-eight ring configuration. The cavity on the left serves as an NOLM. The cavity loss of an NOLM is large at low peak power, but low at high peak power. The output intensity is controlled by the intensity dependent nonlinear phase shift difference between the two arms of the beam splitter [32], thus providing the required mode-locking mechanism. Unlike other figure-eight mode-locked laser configurations, we deployed a resonant nonlinear filter [33] to achieve the required phase shift.

Fig. 42b shows the microscope image of the fabricated 11-th order ring device, and also the SEM picture of the ring cross-section. The dimension of square waveguide core is 1.45 μm x 1.45 μm. The reflective index of the waveguide is 1.7,

which is doped in silica glass.

Configuration

From Fig. 42a, the isolator on the left side loop ensures single direction operation of the loop in the figure-eight laser, i.e. clockwise at left side loop and counter clockwise at the right side loop. A polarization controller by Nufern SM1950 fiber is used to control the polarization. The dispersion of the fiber is about 32 ps/nm/km. In addition, a 1% tap coupler is used as the output port of the circuit. A 2×2 5:95 coupler is used to connect the two loops. In the right loop, a tunable filter (Koshin Kogaku TFM-1800-S-FA) is used to select the specific filter passband used in the experiment. The tunable range of the filter is 10 nm from 1805 to 1815 nm. Thus, the signal will pass through the passband of the nonlinear resonator filter. Fig. 42(b) shows the integrated resonator geometry and a SEM image of the device cross section, respectively. The geometry shows that there are two buses and four ports in the ring. The details of the device can be found in [31]. The input port and drop port are used as the input and output of the nonlinear filter. The output from the through port of the high-order ring resonator was used to monitor the tuning of the filter. The gain is provided by a combination of a 1560 nm pump laser and a Tm-doped nonlinear fiber (Nuferm SM-TSF-9/125) using backward pumping. The total length of

the cavity is about 22 meters, which gives a repetition rate of 9.09 MHz.

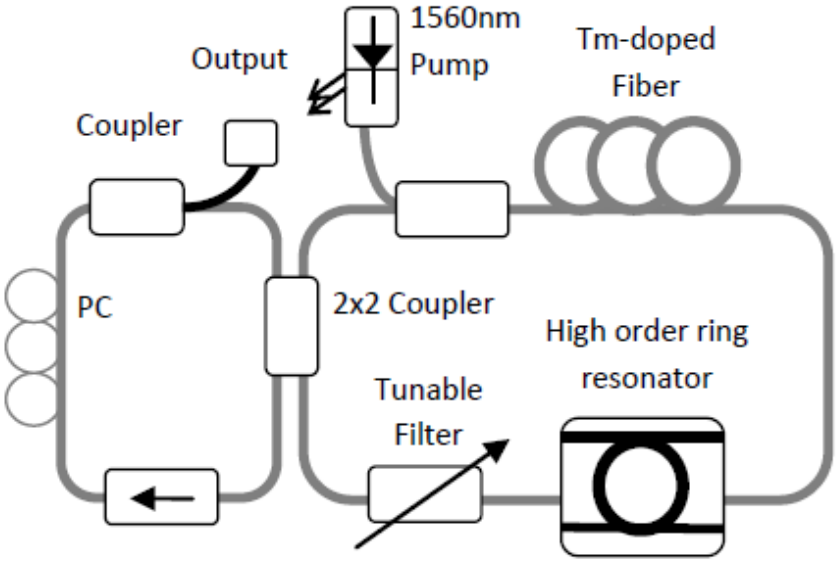

Fig. 42a. Schematic of a ring configuration passive mode-locking optical fiber laser

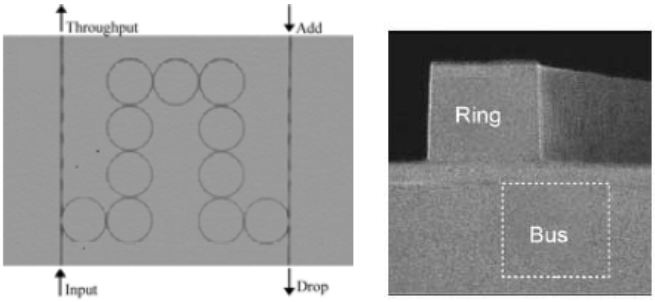

Fig. 42b. Microscope image of the fabricated 11-th order ring device (left). SEM picture of the ring cross-section (right)

The output of the oscillator is then amplified by another Tm-doped amplifier. 20 dBm average output power can be achieved, which is limited by the gain peak at 2 µm, introducing a huge ASE. When the pump power further increases, lasing is achieved at 2 µm.

Experimental results

Fig. 45a shows the linear response of the 11-th ring resonator at 1.81 µm. The bandwidth is approximately 45.5 GHz and FSR is 637 GHz. Fig. 46a shows single pulse operation. Fig. 46b and 46c shows the OSA spectra of the drop port, and the output port respectively.

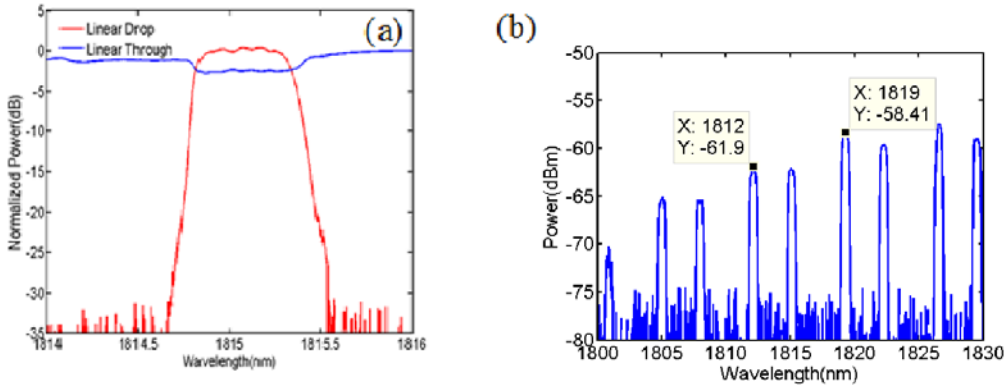

Fig. 45. Linear response of the 11-th ring resonator at 1.8 µm (a) for both the drop and through ports, and the (b) drop port with wider span

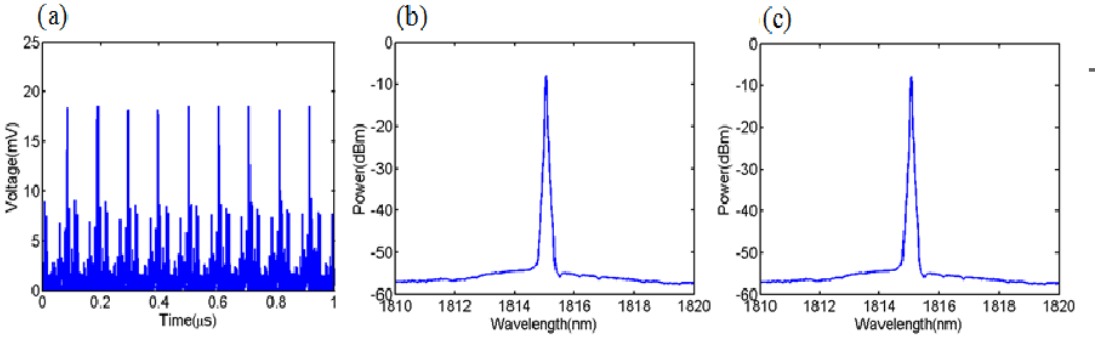

Fig. 46. (a) The timing response measured at output port. The optical spectrum measured at the (b) drop port, and (c) output port.

During the tuning of the laser, we fixed the pump power and carefully varied the orientation of the paddles of the intra-cavity PC to achieve mode-locking. We observed that mode-locking can also be obtained if only the microring filter is used

without the figure-eight configuration. Fig. 47 shows that mode-locking with two-pulse, three-pulse, and six-pulse operations can be achieved. The mock locked pulses however are not stable. Thus stable mode-locking is achieved only by using both the figure-eight laser configuration and the nonlinear ring filter. Also, the wavelength range of the filter limits the longest wavelength of the mode-locked laser at 1.8 μm.

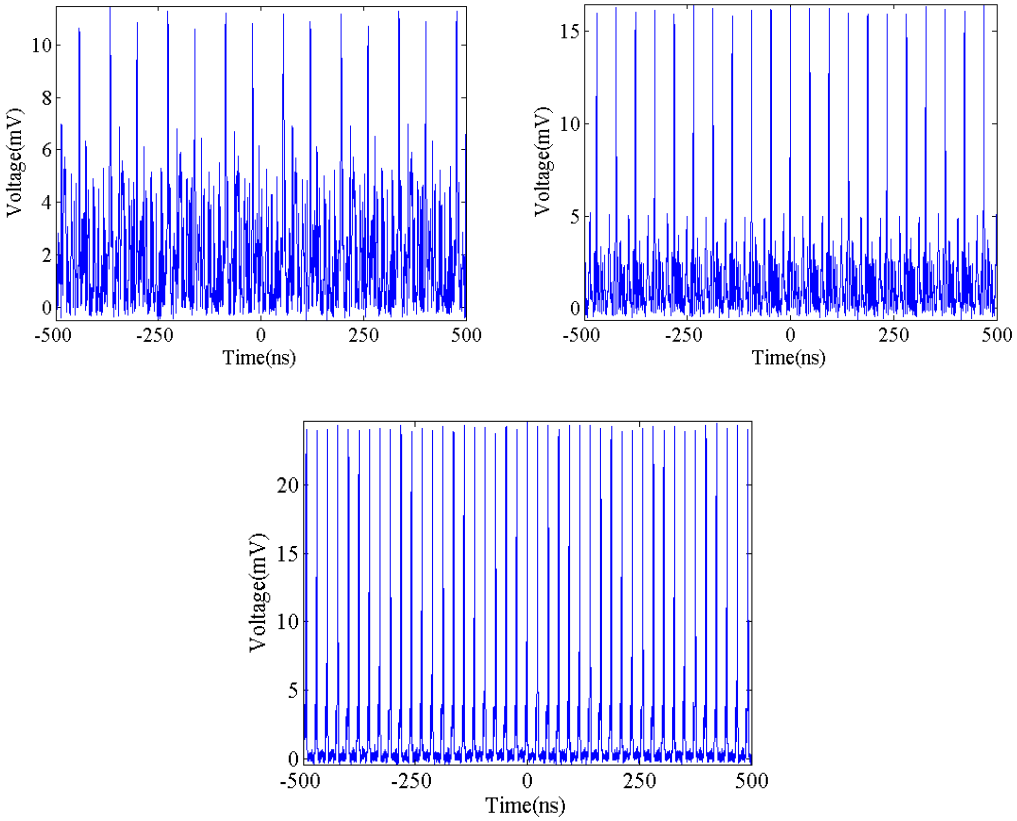

Fig. 47. Two pulses mode operation (top left). Three pulses mode operation (top right). Sixth pulses operation (bottom).

Mode-locking at 1.81 μm was achieved using the figure-eight laser configuration combined with an 11-th order micro-ring resonator. Stable mode-locked pulses with

width of less than 100 ps at 9.09 MHz repetition rate are demonstrated.

Modelling

The figure-eight laser operating in normal dispersion is studied. We use the method in [34-36] by solving the coupled nonlinear Schrödinger (NLS) equations. Only single polarization is taken into account for simplicity. Then,

$$\frac{\partial \mathrm{A}(\xi,\mathrm{T})}{\partial \xi}+\frac{i}{2}\left(\beta^{(2)}+ig\frac{1}{\Omega_g^2}\right)\frac{\partial A(\xi,T)}{\partial T^2}=i\gamma|A(\xi,T)|^2A(\xi,T)+\frac{g}{2}A(\xi,T) \quad , \qquad (16)$$

where A is the field envelope, ξ is the propagation coordinate, T is pulse duration, $\beta^{(2)}$ is the group velocity dispersion, γ is the nonlinear coefficient, and Ω_g is the gain bandwidth. The gain g is given by

$$\mathrm{g}=\frac{\mathrm{g}_0}{(1+\mathrm{P_a}/\mathrm{P_s})} \quad , \qquad (17)$$

where g_0 is the small signal gain, P_s is the saturation power, and P_a is the average power. Here, we assume the effect of the figure-eight can be worked as an SA, which is modeled by the intensity-dependent function T(I),

$$\mathrm{T(I)}=1-\left(\frac{\alpha_0}{(1+\mathrm{I}/\mathrm{I_s})}+\alpha_n\right) \quad , \qquad (18)$$

where I is the pulse intensity, $\mathrm{I_{sat}}$ is the saturation intensity of the SA, α_n is the insertion loss, and α_0 is the modulation depth. The net cavity dispersion $\beta^{(2)}_{net}$ is

$$\beta_{net}^{(2)}=\sum_i L_i\times\beta_i^{(2)} \quad , \qquad (19)$$

where L is the fiber length and i is fiber section. The gain bandwidth of the active fiber, Ωg, is 155 THz. In order to investigate the effect of the fight-eight configuration,

we compare the results with and without SA function.

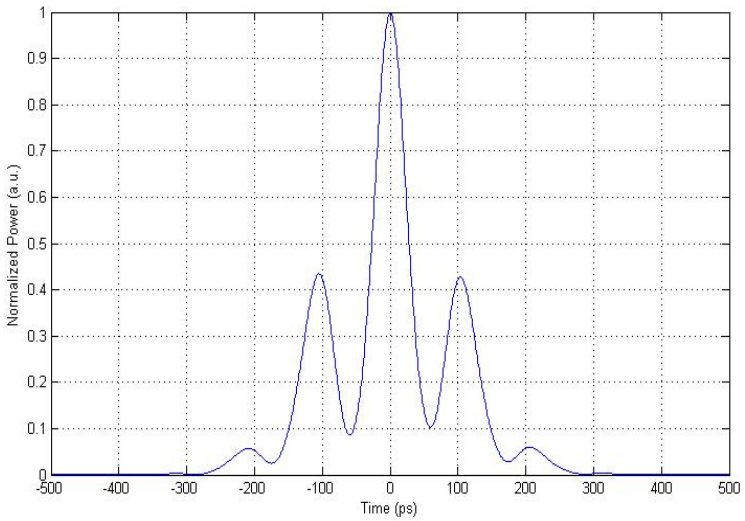

Fig. 48. The simulated results without SA

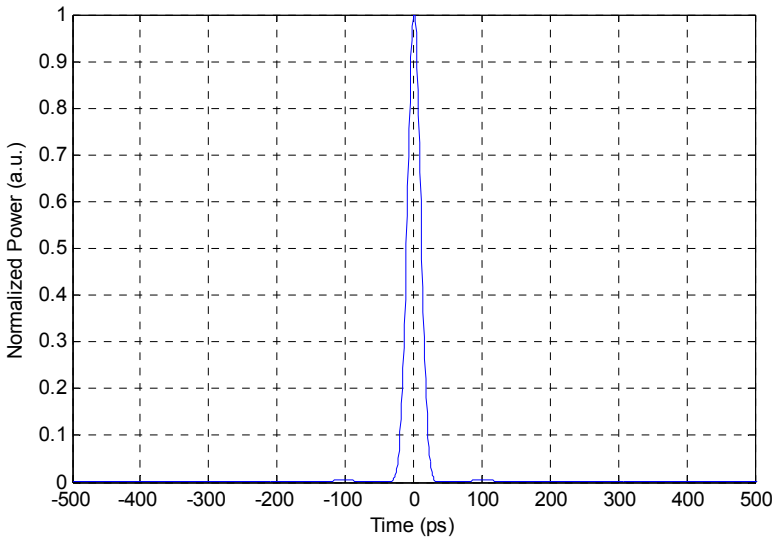

Fig. 49. The simulated results with SA.

Fig. 48 shows the laser pulse without SA. Fig. 49 shows the simulated results with SA. By adjusting the T(I), the side pulses can be compressed. In addition, the simulated results show that the pulse width is around 30-40 ps, which agreed with the experimental measurements.

In the previous section, the pulse width, spectra, and the power of 1550nm

mode-locked laser by using SESAM are measured. Also, the dispersion of the ring resonator is measured. However, it is difficult to measure the 2μm range mode-locked laser pulse shape by using high speed 2 μm detector. It is also difficult to measure the pulse width by using auto-correlator since the existing equipment cannot measure the auto-correlation trace in 2 μm range.

3.3 Conclusion

In this Chapter, mode-locking by using SESAM and microring resonator are demonstrated. In fact, CNT and graphene are also tested. During the experiments, CNT performs similarly to SESAM, however, its stability is not as good as SESAM. The single pulse operation region is narrower than SESAM. Therefore, SESAM is used for further experiments. Graphene can hardly mode-lock. It may be due to the low absorption when compared to CNT and SESAM.

A waveguide ring resonator is used for mode-locking. High Q rings, and different number of higher order rings are used. High Q ring can be achieved by adjusting the coupling ratio from the input to the through port during the manufacturing process. High Q ring cannot perform easily, which may be due to the fact that insertion loss of high Q ring from the input port to the drop port is high. The coupling loss of the waveguide to the fiber port is higher for that high Q ring. As a result, the total loss within the cavity is high. In addition, the coupling loss between the waveguide and the fiber is essential as well. Higher order rings can provide a higher extinction ratio transfer function. It can also reduce mode hopping, allowing stable mode-locking to occur.

Ring resonators are also temperature controlled. For better performance, two level TEC controls are deployed. The lasing center wavelength can be temperature

tuned as well. Both the gain fiber and the passive fiber within the cavity are important. Stable mode-locked laser cannot be achieved if the fibers are not fixed properly.

In microring resonators, the number of microring mainly affects the FSR. The larger number of ring resonators, the higher the FSR. In experiments, we tested different number of microrings, including one, two, three, five, and eleven. It is found that the eleventh order ring resonator achieves the most stable results. Therefore, an eleventh order microring resonator is used in our experimental setup. We believe the stability is related to the coupling loss. One reason is that from simulation results, FSR does not seem to be the significant effect.

In practice, the coupling loss of each microring resonator is difficult to control. The variation of the loss can be more than 3 dB. Further studies on the ring resonator are needed. The effect on different parameters such as number of ring, the coupling loss, operating wavelength range, etc, should be considered. The insertion loss of higher order ring resonator in longer wavelength towards 2 μm is higher than 1.8 μm.

Chapter 4 Summary and future work

In this thesis, we studied high power fiber lasers. First, laser structures and the basic of fiber laser were present. Applications by using fiber lasers are also introduced. In order to achieve high power, MOPA configuration is used, which means a seed laser and an optical power amplifier are needed.

To build a seed laser, we analyzed the characteristics of fiber lasers and demonstrated how to achieve a single polarization single frequency narrow linewidth fiber laser. Measurement of the laser linewidth and noise were performed. We also built CW fiber lasers and pulse lasers by using SESAMs and waveguide ring resonators.

The use of DCF in designing in wide range amplifiers was carried out. In addition, not only DCFs but also LMA DCFs were also studied in order to build a power amplifier in pulse application. A LMA DCF fiber amplifier for LiDAR application in wind speed detection is demonstrated. Measurement by using pre-shaping was considered. Special handling of LMA DCF to ensure single mode operation was also shown.

LMA DCFs with end pumping methods were used. To apply the technology, MFAs and combiners [45, 46] are the key components. Since Yb^{3+} doped fiber lasers

can provide high output power with high power conversion efficiency, they are used to study the power evolution of fiber lasers. In commercial fiber laser products, the current highest output power in CW in single mode can be up to 150 W with single mode fiber output.

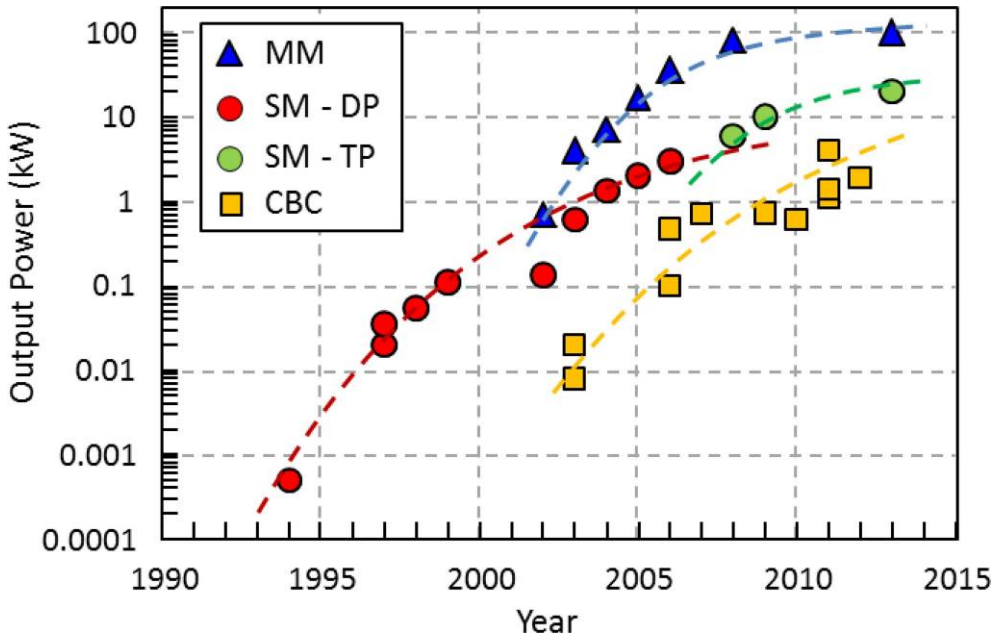

Fig. 49. Power evolution in high-power Yb^{3+} cladding pumped fiber lasers.

The power evolution of Yb^{3+} fiber laser is shown in Fig. 49 [45]. There are four different types of fiber lasers, namely multimode (MM), single mode diode pumped (SM-DP), single mode tandem pumped (SM-TP), and coherent beam combination (CBC) [45]. The growth of output power of multimode fiber lasers slowing down after 2008. The growth of the power is mainly by incoherent combination geometrically.

The current limit is at about the 100 kW level [45].

Advanced fiber technologies including LMA and DCF enhance the growth of the output power. Tandem pumping [47-49], and CBC [45] are new technologies for further increase in the output power.

This thesis does not target to achieve the highest power. It is because we do not have the abilities of design and implementation of high power fiber and fiber components at the moment. Instead, we focus on different new technologies to apply on building specified fiber lasers used in the industry. Therefore, we discussed with commercial suppliers to customize fiber and components.

The following topics are suggested for further studies. First, the measurement and optimization of laser noise. We may consider circuit modification to reduce laser noise. Second, studies on tandem pumping, and CBC should be carried out.

For pulse fiber lasers, we studied how to construct mode-locked fiber lasers by using different technologies. Besides using traditional SESAM, CNT, ring resonators are also adopted. To further study the mode-locking operation by using ring resonators, the effect of different order of rings, and the simulation of figure-eight configuration can be carried out. Simulation work would help analyze the overall operation.

Besides different types of SAs, there are much research work on passive

mode-locked fiber lasers, including dissipative solitons [38], dissipative four-wave mixing [39], and self-induced modulation instability (MI) [40 -42]. The important factors considered are the operating wavelength, the gain bandwidth, fiber length, and particularly the fiber dispersion. Experiments can be carried out in order to achieve the techniques required.

MOPA [51, 52] is used to achieve high pulse energy. Chirped pulse amplification (CPA) [53] is commonly used to compress the pulse during amplification. MOPA with and without CPA can be carried out for high pulse energy applications later on.

In conclusion, fiber laser and fiber amplifier designs are reviewed and studied. The laser characteristics, measurement parameters, and measurement methods are carried out. Some novel ideas and techniques on laser designs, fiber amplifier operations, and implementations are demonstrated.

Fiber laser systems have many applications, especially in sensing areas. Industrial use of fiber lasers will be increasingly important since fiber lasers can provide a good beam quality with compact size and reasonable price.

However, industrial standards for fiber lasers are not established at the moment. In comparison, traditional electrical sensors, such as strain gage in sensing systems, are commonly used, and easy to apply in the monitoring and control system because they are standardized. Fiber sensors and fiber lasers should also be standardized to

allow side adoption by industries.

References

[1] E.Snitzer, “Optical Maser Action of Nd+3 in a Barium Crown Glass”, Phys. Rev. Lett 7444(1961)

[2] Shenghong Huang, Guanshi Qin, Akira Shirakawa, Mitsuru Musha and Ken-ichi Ueda, “Single frequency 1083nm ytterbium doped fiber master oscillator power amplifier laser”, Optics Express, Vol.13, No.18, p.7113-7117(2005)

[3] Shenghong Huang, Guanshi Qin, Akira Shirakawa, Mitsuru Musha and Ken-ichi Ueda, “Single frequency fiber laser from linear cavity with loop mirror filter and dual cascaded FBGs.”, IEEE Photonics Technology Letter Vol.17, No.6, p.1169-1171(2005)

[4]Alexander Polynkin, Pavel Polynkin, Masud Mansuripur, N. Peyghambarian, “Single frequency fiber ring laser with 1W output power at 1.5um”, Optics Express, Vol 13, No.8, p.3179-3184 (2005)

[5] Huang Shenghong, “Single frequency ytterbium fiber laser and phosphosilicate Raman fiber laser”, 2006

[6] Zhou meng, George Stewart, Gillian Whitenett, “Stable Single Mode Operation of a Narrow Linewidth, Linearly Polarized, Erbium Fiber Ring Laser Using a Saturable Absorber”, IEEE Journal of Lightwave Technology, Vol 24, no. 5,

p2179-2183(2006)

[7] R. Paschotta, J. Nilsson, L. Reekie, A. C. Trooper, D.C. Hanna, “Single-frequency ytterbium-doped fiber laser stabilized by spatial hole burning”, Optics Letters, Vol. 22, No. 1, (1997)

[8]Yuichi Takushima, Shinji Yamashita, Kazuro Kikuchi, Kazuo Hotate, “Polariztion Stable and Single Frequency Fiber Laser”, IEEE Journal of Lighwave Technology, Vol 16, No 4, p.661-669(1998)

[9] Hajime Inaba, Yoshiaki Akimoto, Koichi Tamura, Eiji Yoshida, Tetsuro Komukai, Masataka Nakazawa, “A Single-Frequency and Single-Polarization Fiber Ring Laser Using a 5 GHz Fiber Bragg Grating”, Electronics and Communications in Japan, Part 2, Vol 82, No5, (1999)

[10] Malinowski, A., et al. "Pulsed high power fiber laser systems." LEOS Summer Topical Meetings, 2006 Digest of the. IEEE, 2006.

[11] Samson, Bryce, et al. "High-Power Large-Mode Area Optical Fibers for Fiber Lasers and Amplifiers." Optical Fiber Communication Conference. Optical Society of America, 2008.

[12] S. Grot, et al., “High power Yb3+-doped double clad fibre amplification at 1127 nm: 977 against 920nm pumping comparison”, Electronics Letters, 16, vol. 39 No. 21.

[13] H.M. Pask, et al, “Ytterbium-Doped Silica Fiber Lasers: Versatile Sources for the 1-1.2um Region”, IEEE J. Quantum Electron, 1,1 (1995)

[14] Paschotta R., et al., “Ytterbium-doped fiber amplifiers”, IEEE J.Quantum Electron., 33, 7 (1997)

[15] Sylvain Bordais, et al, “Double-clad 10-W Y3+-doped fiber master oscillator power fiber amplifier for He3 optical pumping”, Applied Optics, 43, 10, 2188-2174.

[16] Knight, J. C., et al. "All-silica single-mode optical fiber with photonic crystal cladding." Optics letters 21.19 (1996): 1547-1549.

[17] Carter, Adrian. "Optical fibers for high-power eye-safe lasing applications."

[18] Liem, A., et al. "100-W single-frequency master-oscillator fiber power amplifier." Optics Letters 28.17 (2003): 1537-1539.

[19] J. Limpert, T. Schreiber, T. Clausnitzer, K. Zöllner, H. -. Fuchs, E. -. Kley, H. Zellmer, and A. Tünnermann, "High-power femtosecond Yb-doped fiber amplifier," Opt. Express 10, 628-638 (2002).

[20] J.A. Alvarez-Chavez, A.B. Grudinin, J. Nilsson, P.W. Turner, and W.A. Clarkson, “Mode selection in high power cladding pumped fiber lasers with tapered sections,” in Conference on Lasers and Electro-Optics, Optical Society of America, Washighton, D.C., 1999, page 247.

[21] J. Sakai and T. Kimura, “Bending loss of propagation modes in arbitrary-index profile optical fibers,” Appl. Opt. 17, 1499 (1978).

[22] Limpert, Jens, et al. "The rising power of fiber lasers and amplifiers." Selected Topics in Quantum Electronics, IEEE Journal of 13.3 (2007): 537-545.

[23] M.E. Fermann, “Single-mode excitation of multimode fibers with ultrashort pulses,” Opt. Lett. 23, 52 (1998).

[24] Ippen, E. P., L. Y. Liu, and H. A. Haus. "Self-starting condition for additive-pulse mode-locked lasers." Optics letters 15.3 (1990): 183-185.

[25] Yamashita, Shinji, Amos Martinez, and Kin Kee Chow. "Application of carbon nanotubes for mode-locked fiber lasers and nonlinear devices." OptoElectronics and Communications Conference, 2009. OECC 2009. 14th. IEEE, 2009.

[26] Sun, Z., T. Hasan, and A. C. Ferrari. "Ultrafast lasers mode-locked by nanotubes and graphene." Physica E: Low-dimensional Systems and Nanostructures 44.6 (2012): 1082-1091.

[27] S. Zhang, F. Lu, X. Dong, P. Shum, X. Yang, X. Zhou, Y. Gong, and C. Lu, “Passive mode-locking at harmonics of the free spectral range of the intracavity filter in a fiber ring laser,” Opt. Lett. 30 (2005) p. 2852

[28] L. Razzari, D. Duchesne, M. Ferrera, R. Morandotti, S. T. Chu, B. E. Little and D. J. Moss, “CMOS-compatible integrated optical hyper-parametric oscillator,” Nature

Photon. 4 (2010) p. 41

[29] Jin, Li, et al. "Burst-mode operation of a 650GHz mode-locked laser based on a high order microring resonator." OptoElectronics and Communications Conference (OECC) 2014.

[30] P. Grelu and N.Akhmediev, “Dissipative solitons for mode-locked lasers,” Nature Photonics 6 (2012) p. 84

[31] M. Peccianti, A. Pasquazi,Y. Park, B.E. Little, S.T. Chu, D.J. Moss and R. Morandotti, “Demonstration of a stable ultrafast laser based on a nonlinear microcavity”, Nat. Commun. 3 (2012) p. 765

[32] Rudy, Charles W., et al. "Amplified 2-μm thulium-doped all-fiber mode-locked figure-eight laser." Journal of Lightwave Technology 31.11 (2013): 1809-1812.

[33] Geuzebroek, Douwe H., and Alfred Driessen. "Ring-resonator-based wavelength filters." Wavelength filters in fibre optics. Springer Berlin Heidelberg, 2006. 341-379.

[34] Liu, H. H., and K. K. Chow. "Enhanced stability of dispersion-managed mode-locked fiber lasers with near-zero net cavity dispersion by high-contrast saturable absorbers." Optics letters 39.1 (2014): 150-153.

[35] Fedotov, Y. S., et al. "High average power mode-locked figure-eight Yb fibre master oscillator." Optics express 22.25 (2014): 31379-31386.

[36] Li, Huihui, et al. "Pulse-shaping mechanisms in passively mode-locked thulium-doped fiber lasers." Optics express 23.5 (2015): 6292-6303.

[37] Xia, Fengnian, et al. "Ultra-compact high order ring resonator filters using submicron silicon photonic wires for on-chip optical interconnects." Optics express 15.19 (2007): 11934-11941.

[38] P. Grelu and N.Akhmediev, “Dissipative solitons for mode-locked lasers,” Nature Photonics 6 (2012) p. 84

[39] M. Quiroga-Teixeiro, C. B. Clausen, M. P. Sørensen, P. L. Christiansen, and P. a. Andrekson, “Passive mode-locking by dissipative four-wave mixing,” J. Opt. Soc. Am. 15 (1998) p.1315

[40] P. Franco, F. Fontana, I. Cristiani, M. Midrio, and M. Romagnoli, “Self-induced modulational-instability laser,” Opt. Lett. 20 (1995) p. 2009

[41] E. Yoshida and M. Nakazawa, “Low-threshold 115-GHz continuous-wave modulational-instability erbium-doped fiber laser,” Opt. Lett. 22 (1997) p. 1409

[42] T. Sylvestre, S. Coen, P. Emplit, and M. Haelterman, “Self-induced modulational instability laser revisited: normal dispersion and dark-pulse train generation,” Opt. Lett. (2002) p. 482

[43] J. Schröder, T. D. Vo, and B. J. Eggleton, “Repetitionrate-selective, wavelength-tunable mode-locked laser at up to 640 GHz,” Opt. Lett. 34 (2009) p.

3902

[44] J. Schröder, D. Alasia, T. Sylvestre, and S. Coen, “Dynamics of an ultrahigh-repetition-rate passively modelocked Raman fiber laser,” J. Opt. Soc. Am. 25 (2008) p. 1178

[45] Zervas, Michalis N., and Christophe A. Codemard. "High power fiber lasers: a review." Selected Topics in Quantum Electronics, IEEE Journal of 20.5 (2014): 219-241.

[46] Zhou, Xuanfeng, et al. "Mode-field adaptor between large-mode-area fiber and single-mode fiber based on fiber tapering and thermally expanded core technique." Applied optics 53.22 (2014): 5053-5057.

[47] Neugroschl, Dan, et al. "High-efficiency (6+ 1) x1 combiner for high power fiber lasers and amplifiers." SPIE LASE. International Society for Optics and Photonics, 2013.

[48] O’Connor, Michael, and Bill Shiner. "High power fiber lasers for industry and defense." Chap 18 (2011): 517-532.

[49] Zhu, Jiajian, et al. "Power scaling analysis of tandem-pumped Yb-doped fiber lasers and amplifiers." Optics express 19.19 (2011): 18645-18654.

[50] Su, Rongtao, et al. "Active coherent beam combination of two high-power single-frequency nanosecond fiber amplifiers." Optics letters 37.4 (2012):

497-499.

[51] Liu, Jiang, Qian Wang, and Pu Wang. "High average power picosecond pulse generation from a thulium-doped all-fiber MOPA system." Optics express 20.20 (2012): 22442-22447.

[52] Liu, Jiang, et al. "High average power picosecond pulse and supercontinuum generation from a thulium-doped, all-fiber amplifier." Optics letters 38.20 (2013): 4150-4153.

[53] Haxsen, Frithjof, et al. "Pulse energy of 151 nJ from ultrafast thulium-doped chirped-pulse fiber amplifier." Optics letters 35.17 (2010): 2991-2993.